SANDIA REPORT
SAND2004-4816
Unlimited Release
Printed October 2004

A Set of Verification Test Cases for Eiger: Plane Wave Scattering from a Sphere

Roy E. Jorgenson and Joseph D. Kotulski

Prepared by
Sandia National Laboratories
Albuquerque, New Mexico 87185 and Livermore, California 94550

Sandia is a multiprogram laboratory operated by Sandia Corporation,
a Lockheed Martin Company, for the United States Department of Energy's
National Nuclear Security Administration under Contract DE-AC04-94AL85000.

Issued by Sandia National Laboratories, operated for the United States Department of Energy by Sandia Corporation.

Available to DOE and DOE contractors from
U.S. Department of Energy
Office of Scientific and Technical Information
P.O. Box 62
Oak Ridge, TN 37831

Telephone: (865)576-8401
Facsimile: (865)576-5728
E-Mail: reports@adonis.osti.gov
Online ordering: http://www.osti.gov/bridge

Available to the public from
U.S. Department of Commerce
National Technical Information Service
5285 Port Royal Rd
Springfield, VA 22161

Telephone: (800)553-6847
Facsimile: (703)605-6900
E-Mail: orders@ntis.fedworld.gov
Online order: http://www.ntis.gov/help/ordermethods.asp?loc=7-4-0#online

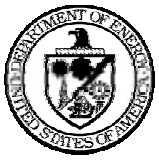

SAND2004-4816
Unlimited Release
Printed October 2004

A Set of Verification Test Cases for Eiger: Plane Wave Scattering from a Sphere

Roy E. Jorgenson and Joseph D. Kotulski
Electromagnetics and Plasma Physics Analysis Dept.
Sandia National Laboratories
P. O. Box 5800
Albuquerque, NM 87185-1152

Abstract

This report discusses a set of verification test cases for the frequency-domain, boundary-element, electromagnetics code **Eiger** based on the analytical solution of plane wave scattering from a sphere. Three cases will be considered: when the sphere is made of perfect electric conductor, when the sphere is made of lossless dielectric and when the sphere is made of lossy dielectric. We outline the procedures that must be followed in order to carefully compare the numerical solution to the analytical solution. We define an error criterion and demonstrate convergence behavior for both the analytical and numerical cases. These problems test the code's ability to calculate the surface current density and secondary quantities, such as near fields and far fields.

Contents

Figures

Intentionally Left Blank

A Set of Verification Test Cases for Eiger: Plane Wave Scattering from a Sphere

1 Introduction

In this report we compare solutions obtained from the frequency-domain, boundary-element, electromagnetics code **Eiger** to analytical solutions of plane wave scattering from a sphere. Three types of spheres will be considered: a perfect electric conductor (PEC), lossless dielectric and lossy dielectric.

We begin by defining the general test case geometry. We then derive the analytical solution of plane wave scattering from a PEC sphere and calculate all components of both E and H fields in spherical coordinates at locations outside the sphere. By allowing the observation point to be on the surface of the sphere, we obtain both components of electrical current density, which are the principal unknowns calculated by **Eiger**. By allowing the radius of the observation point to approach infinity, we obtain the E field components in the far field. In Section 3.4, we perform a convergence study of the analytical solution for all quantities calculated. The procedures used to compare the numerical solution to the analytical solution are quite involved and are, therefore, documented in Section 3.5. Comparisons between numerical and analytical solutions are made for all quantities at various frequencies to show how the error varies as a function number of basis functions per wavelength. Results are shown for the three equations that are implemented in **Eiger** to solve the PEC boundary condition: the electric field integral equation (EFIE), the magnetic field integral equation (MFIE) and the combined field integral equation (CFIE). We also demonstrate how the CFIE overcomes problems that the EFIE and MFIE have at internal resonance. Comparing results of **Eiger** to the analytical calculation of currents on the PEC sphere is one of the verification tests required for the electromagnetic radiation (EMR) environment (Test 1.a.a) [1].

The analytic solution to plane wave scattering from a dielectric sphere is discussed in Section 4. Convergence studies, comparison procedures and comparisons to numerical solutions follow the same format as the PEC sphere. The lossy dielectric sphere discussion starts in Section 5 and follows the same format as the other two test cases.

2 Test Case Geometry

Consider a plane wave travelling in the $+\widehat{z}$ direction incident on a sphere as shown in Figure 1. The $\overrightarrow{E}$ field is polarized along $\widehat{x}$ so

$$\overrightarrow{E} = \widehat{x} E_0 e^{-jk_0 z}$$

where $k_0 = \omega\sqrt{\varepsilon_0 \mu_0}$ is the wavenumber in free-space (throughout this report, we assume an $e^{+j\omega t}$ time dependency). The sphere is centered at the origin and has a radius a.

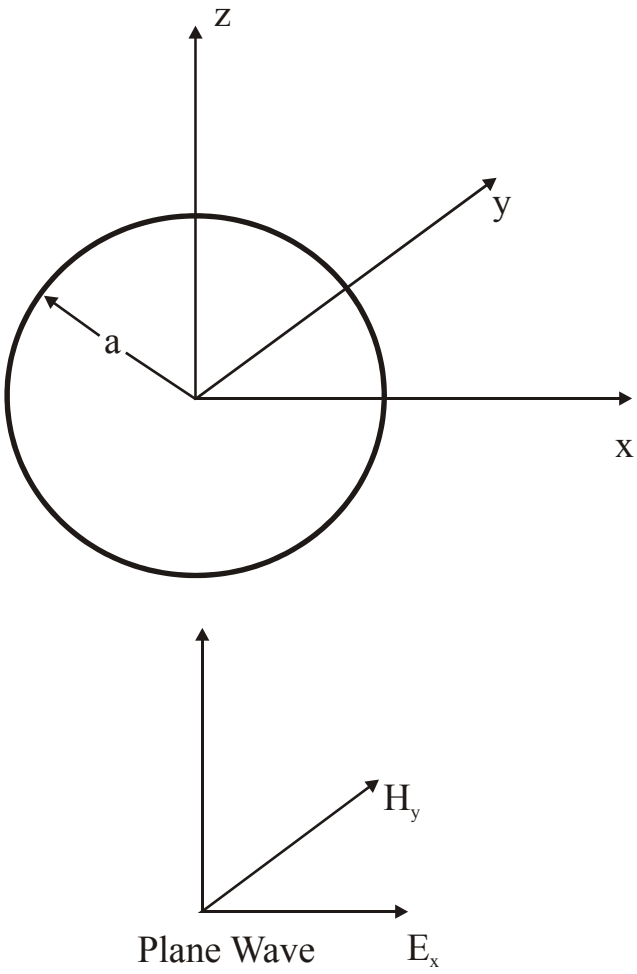

Figure 1. Plane wave incident on a sphere

3 PEC Sphere Test Case

3.1 Derivation of the Analytical Solution

If the sphere is a PEC, the potentials at $r \geq a$ are given as [2]

$$A_r^+ = \frac{E_0}{\omega\mu_0}\cos\phi \sum_{n=1}^{\infty}\left[a_n \widehat{J}_n\left(k_0 r\right) + b_n \widehat{H}_n^{(2)}\left(k_0 r\right)\right] P_n^1\left(\cos\theta\right)$$

$$F_r^+ = \frac{E_0}{k_0}\sin\phi \sum_{n=1}^{\infty}\left[a_n \widehat{J}_n\left(k_0 r\right) + c_n \widehat{H}_n^{(2)}\left(k_0 r\right)\right] P_n^1\left(\cos\theta\right)$$

where r, θ and ϕ are the spherical coordinates; P_n^1 is the associated Legendre polynomial of order 1 and degree n; $\widehat{J_n}$ is the alternative spherical Bessel function of the first kind, order n; $\widehat{H}_n$ is the alternative spherical Hankel function of the second kind, order n; and μ_0 is the permeability of the medium surrounding the sphere. Calculation of P_n^1, $\widehat{J}_n$ and $\widehat{H}_n$, along with their derivatives, are discussed in Appendix I.

Additionally,

$$a_n = \frac{j^{-n}\left(2n+1\right)}{n\left(n+1\right)}$$
$$b_n = -a_n \frac{\widehat{J}_n'\left(k_0 a\right)}{\widehat{H}_n^{(2)\prime}\left(k_0 a\right)}$$
$$c_n = -a_n \frac{\widehat{J}_n\left(k_0 a\right)}{\widehat{H}_n^{(2)}\left(k_0 a\right)}$$

The total field components are calculated from these potentials. For the E field components

$$\begin{aligned}
E_r &= \frac{1}{j\omega\varepsilon_0}\left(\frac{\partial^2}{\partial r^2}+k_0^2\right)A_r^+ \\
&= \frac{-jE_0}{\omega^2\varepsilon_0\mu_0}\cos\phi\sum_{n=1}^{\infty}\left[a_n\left(\frac{\partial^2}{\partial r^2}+k_0^2\right)\widehat{J}_n\left(k_0 r\right)+b_n\left(\frac{\partial^2}{\partial r^2}+k_0^2\right)\widehat{H}_n^{(2)}\left(k_0 r\right)\right]P_n^1\left(\cos\theta\right) \\
&= -jE_0\cos\phi\sum_{n=1}^{\infty}\left[a_n\widehat{J}_n''\left(k_0 r\right)+b_n\widehat{H}_n^{(2)\prime\prime}\left(k_0 r\right)\right]P_n^1\left(\cos\theta\right)+\left[a_n\widehat{J}_n\left(k_0 r\right)+b_n\widehat{H}_n^{(2)}\left(k_0 r\right)\right]P_n^1\left(\cos\theta\right)
\end{aligned}$$

$$\begin{aligned}
E_\theta &= \frac{-1}{r\sin\theta}\frac{\partial F_r^+}{\partial\phi}+\frac{1}{j\omega\varepsilon_0 r}\frac{\partial^2 A_r^+}{\partial r\partial\theta} \\
&= \frac{-E_0}{rk_0\sin\theta}\frac{\partial}{\partial\phi}\left(\sin\phi\right)\sum_{n=1}^{\infty}\left[a_n\widehat{J}_n\left(k_0 r\right)+c_n\widehat{H}_n^{(2)}\left(k_0 r\right)\right]P_n^1\left(\cos\theta\right) \\
&\quad +\frac{-jE_0}{\omega^2\mu_0\varepsilon_0 r}\left[\cos\phi\sum_{n=1}^{\infty}\frac{\partial}{\partial r}\left[a_n\widehat{J}_n\left(k_0 r\right)+b_n\widehat{H}_n^{(2)}\left(k_0 r\right)\right]\frac{\partial}{\partial\theta}\left(P_n^1\left(\cos\theta\right)\right)\right] \\
&= \frac{-E_0\cos\phi}{k_0 r}\sum_{n=1}^{\infty}\left[a_n\widehat{J}_n\left(k_0 r\right)+c_n\widehat{H}_n^{(2)}\left(k_0 r\right)\right]\frac{P_n^1\left(\cos\theta\right)}{\sin\theta}-j\left[a_n\widehat{J}_n'\left(k_0 r\right)+b_n\widehat{H}_n^{(2)\prime}\left(k_0 r\right)\right]P_n^{1\prime}\left(\cos\theta\right)\sin\theta
\end{aligned}$$

At $r=a$, and substituting for b_n and $\dot{c}_n$ in terms of a_n we obtain

$$\begin{aligned}
E_\theta &= \frac{-E_0\cos\phi}{k_0 a}\sum_{n=1}^{\infty}\left[a_n\widehat{J}_n\left(k_0 a\right)-a_n\frac{\widehat{J}_n\left(k_0 a\right)}{\widehat{H}_n^{(2)}\left(k_0 a\right)}\widehat{H}_n^{(2)}\left(k_0 a\right)\right]\frac{P_n^1\left(\cos\theta\right)}{\sin\theta} \\
&\quad -j\left[a_n\widehat{J}_n'\left(k_0 a\right)-a_n\frac{\widehat{J}_n'\left(k_0 a\right)}{\widehat{H}_n^{(2)\prime}\left(k_0 a\right)}\widehat{H}_n^{(2)\prime}\left(k_0 a\right)\right]P_n^{1\prime}\left(\cos\theta\right)\sin\theta \\
&= \frac{-E_0\cos\phi}{k_0 a}\sum_{n=1}^{\infty}\left[0\right]\frac{P_n^1\left(\cos\theta\right)}{\sin\theta}-j\left[0\right]P_n^{1\prime}\left(\cos\theta\right)\sin\theta \\
&= 0
\end{aligned}$$

which states that the PEC boundary condition (E tangential to a PEC surface is zero) is satisfied. The scattered E_θ field is

$$E_\theta^s = \frac{-E_0\cos\phi}{k_0 r}\sum_{n=1}^{\infty}\left[c_n\widehat{H}_n^{(2)}\left(k_0 r\right)\right]\frac{P_n^1\left(\cos\theta\right)}{\sin\theta}-j\left[b_n\widehat{H}_n^{(2)\prime}\left(k_0 r\right)\right]P_n^{1\prime}\left(\cos\theta\right)\sin\theta$$

which, when $kr\to\infty$, becomes

$$\begin{aligned}
E_\theta^s &= \frac{-E_0\cos\phi}{k_0 r}\sum_{n=1}^{\infty}\left[c_n j^{n+1}e^{-jk_0 r}\right]\frac{P_n^1\left(\cos\theta\right)}{\sin\theta}-j\left[b_n j^{n+1}\left(-j\right)e^{-jk_0 r}\right]P_n^{1\prime}\left(\cos\theta\right)\sin\theta \\
&= \frac{jE_0}{k_0 r}e^{-jk_0 r}\cos\phi\sum_{n=1}^{\infty}j^n\left\{b_n P_n^{1\prime}\left(\cos\theta\right)\sin\theta-c_n\frac{P_n^1\left(\cos\theta\right)}{\sin\theta}\right\}
\end{aligned}$$

The total E_ϕ field is

$$\begin{aligned}
E_\phi &= \frac{1}{r}\frac{\partial F_r^+}{\partial\theta} + \frac{1}{j\omega\varepsilon_0 r\sin\theta}\frac{\partial^2 A_r^+}{\partial r\partial\phi} \\
&= \frac{E_0\sin\phi}{rk_0}\sum_{n=1}^{\infty}\left[a_n\widehat{J}_n\left(k_0r\right)+c_n\widehat{H}_n^{(2)}\left(k_0r\right)\right]\frac{\partial}{\partial\theta}\left(P_n^1\left(\cos\theta\right)\right) \\
&\quad -\frac{jE_0}{k_0^2 r\sin\theta}\left[\frac{\partial}{\partial\phi}\left(\cos\phi\right)\sum_{n=1}^{\infty}\frac{\partial}{\partial r}\left[a_n\widehat{J}_n\left(k_0r\right)+b_n\widehat{H}_n^{(2)}\left(k_0r\right)\right]P_n^1\left(\cos\theta\right)\right] \\
&= \frac{-E_0\sin\phi}{k_0r}\sum_{n=1}^{\infty}\left[a_n\widehat{J}_n\left(k_0r\right)+c_n\widehat{H}_n^{(2)}\left(k_0r\right)\right]P_n^{1\prime}\left(\cos\theta\right)\sin\theta - j\left[a_n\widehat{J}_n'\left(k_0r\right)+b_n\widehat{H}_n^{(2)\prime}\left(k_0r\right)\right]\frac{P_n^1\left(\cos\theta\right)}{\sin\theta}
\end{aligned}$$

At $r=a$, the PEC boundary condition states that total $E_\phi=0$, i.e.,

$$\begin{aligned}
E_\phi &= \frac{-E_0\sin\phi}{k_0a}\sum_{n=1}^{\infty}\left[a_n\widehat{J}_n\left(k_0a\right)-a_n\frac{\widehat{J}_n\left(k_0a\right)}{\widehat{H}_n^{(2)}\left(k_0a\right)}\widehat{H}_n^{(2)}\left(k_0a\right)\right]P_n^{1\prime}\left(\cos\theta\right)\sin\theta \\
&\quad -j\left[a_n\widehat{J}_n'\left(k_0a\right)-a_n\frac{\widehat{J}_n'\left(k_0a\right)}{\widehat{H}_n^{(2)\prime}\left(k_0a\right)}\widehat{H}_n^{(2)\prime}\left(k_0a\right)\right]\frac{P_n^1\left(\cos\theta\right)}{\sin\theta} \\
&= 0
\end{aligned}$$

The scattered E_ϕ field is

$$E_\phi^s = \frac{-E_0\sin\phi}{k_0r}\sum_{n=1}^{\infty}\left[c_n\widehat{H}_n^{(2)}\left(k_0r\right)\right]P_n^{1\prime}\left(\cos\theta\right)\sin\theta - j\left[b_n\widehat{H}_n^{(2)\prime}\left(k_0r\right)\right]\frac{P_n^1\left(\cos\theta\right)}{\sin\theta}$$

which, when $kr\to\infty$, becomes

$$\begin{aligned}
E_\phi^s &= \frac{-E_0\sin\phi}{k_0r}\sum_{n=1}^{\infty}\left[c_nj^{n+1}e^{-jk_0r}\right]P_n^{1\prime}\left(\cos\theta\right)\sin\theta - j\left[b_nj^{n+1}\left(-j\right)e^{-jk_0r}\right]\frac{P_n^1\left(\cos\theta\right)}{\sin\theta} \\
&= \frac{jE_0}{k_0r}e^{-jk_0r}\sin\phi\sum_{n=1}^{\infty}j^n\left\{b_n\frac{P_n^1\left(\cos\theta\right)}{\sin\theta}-c_nP_n^{1\prime}\left(\cos\theta\right)\sin\theta\right\}
\end{aligned}$$

The H field components are

$$\begin{aligned}
H_r &= \frac{1}{j\omega\mu_0}\left(\frac{\partial^2}{\partial r^2}+k_0^2\right)F_r^+ \\
&= \frac{-j\sqrt{\varepsilon_0}E_0}{\sqrt{\mu_0}\omega\sqrt{\mu_0\varepsilon_0}k_0}\sin\phi\sum_{n=1}^{\infty}\left[a_n\left(\frac{\partial^2}{\partial r^2}+k_0^2\right)\widehat{J}_n\left(k_0r\right)+c_n\left(\frac{\partial^2}{\partial r^2}+k_0^2\right)\widehat{H}_n^{(2)}\left(k_0r\right)\right]P_n^1\left(\cos\theta\right) \\
&= \frac{-jE_0}{\eta_0}\sin\phi\sum_{n=1}^{\infty}\left[a_n\widehat{J}_n''\left(k_0r\right)+c_n\widehat{H}_n^{(2)\prime\prime}\left(k_0r\right)\right]P_n^1\left(\cos\theta\right)+\left[a_n\widehat{J}_n\left(k_0r\right)+c_n\widehat{H}_n^{(2)}\left(k_0r\right)\right]P_n^1\left(\cos\theta\right)
\end{aligned}$$

$$
\begin{aligned}
H_\theta &= \frac{1}{r\sin\theta}\frac{\partial A_r^+}{\partial\phi}+\frac{1}{j\omega\mu_0 r}\frac{\partial^2 F_r^+}{\partial r\partial\theta} \\
&= \frac{E_0}{\omega\mu_0 r\sin\theta}\left[\frac{\partial}{\partial\phi}(\cos\phi)\sum_{n=1}^{\infty}\left[a_n\widehat{J}_n(k_0r)+b_n\widehat{H}_n^{(2)}(k_0r)\right]P_n^1(\cos\theta)\right] \\
&\quad +\frac{E_0}{j\omega\mu_0 r k_0}\left[\sin\phi\sum_{n=1}^{\infty}\frac{\partial}{\partial r}\left[a_n\widehat{J}_n(k_0r)+c_n\widehat{H}_n^{(2)}(k_0r)\right]\frac{\partial}{\partial\theta}\left(P_n^1(\cos\theta)\right)\right] \\
&= \frac{-E_0\sin\phi}{\eta_0 k_0 r}\sum_{n=1}^{\infty}\left[a_n\widehat{J}_n(k_0r)+b_n\widehat{H}_n^{(2)}(k_0r)\right]\frac{P_n^1(\cos\theta)}{\sin\theta}-j\left[a_n\widehat{J}_n'(k_0r)+c_n\widehat{H}_n^{(2)\prime}(k_0r)\right]P'(\cos\theta)\sin\theta
\end{aligned}
$$

At $r=a$,

$$
\begin{aligned}
H_\theta &= \frac{-E_0\sin\phi}{\eta_0 k_0 a}\sum_{n=1}^{\infty}\left[a_n\widehat{J}_n(k_0a)-a_n\frac{\widehat{J}_n'(k_0a)}{\widehat{H}_n^{(2)\prime}(k_0a)}\widehat{H}_n^{(2)}(k_0a)\right]\frac{P_n^1(\cos\theta)}{\sin\theta} \\
&\quad -j\left[a_n\widehat{J}_n'(k_0a)-a_n\frac{\widehat{J}_n(k_0a)}{\widehat{H}_n^{(2)}(k_0a)}\widehat{H}_n^{(2)\prime}(k_0a)\right]P'(\cos\theta)\sin\theta \\
&= \frac{-E_0\sin\phi}{\eta_0 k_0 a}\sum_{n=1}^{\infty}a_n\left\{\begin{array}{l}\left[\widehat{J}_n(k_0a)\widehat{H}_n^{(2)\prime}(k_0a)-\widehat{J}_n'(k_0a)\widehat{H}_n^{(2)}(k_0a)\right]\frac{P_n^1(\cos\theta)}{\widehat{H}_n^{(2)\prime}(k_0a)\sin\theta} \\ -\left[\widehat{J}_n(k_0a)\widehat{H}_n^{(2)\prime}(k_0a)-\widehat{J}_n'(k_0a)\widehat{H}_n^{(2)}(k_0a)\right]\frac{P'(\cos\theta)\sin\theta}{j\widehat{H}_n^{(2)}(k_0a)}\end{array}\right\}
\end{aligned}
$$

Simplifying the quantities in the brackets by invoking the Wronskian $\left(W=\widehat{J}\widehat{H}'-\widehat{J}'\widehat{H}=-j\right)$ we obtain

$$
\begin{aligned}
H_\theta(k_0a) &= \frac{-E_0\sin\phi}{\eta_0 k_0 a}\sum_{n=1}^{\infty}a_n\left\{[-j]\frac{P_n^1(\cos\theta)}{\widehat{H}_n^{(2)\prime}(k_0a)\sin\theta}-[-j]\frac{P'(\cos\theta)\sin\theta}{j\widehat{H}_n^{(2)}(k_0a)}\right\} \\
&= \frac{j}{\eta_0}E_0\frac{\sin\phi}{k_0a}\sum_{n=1}^{\infty}a_n\left\{\frac{P_n^1(\cos\theta)}{\widehat{H}_n^{(2)\prime}(k_0a)\sin\theta}-\frac{P'(\cos\theta)\sin\theta}{j\widehat{H}_n^{(2)}(k_0a)}\right\}
\end{aligned}
$$

which allows us to calculate the $\widehat{\phi}$ directed electric current density:

$$
\begin{aligned}
\widehat{\phi}J_\phi &= \widehat{r}\times\widehat{\theta}H_\theta \qquad (1)\\
J_\phi &= \frac{j}{\eta_0}E_0\frac{\sin\phi}{k_0a}\sum_{n=1}^{\infty}a_n\left\{\frac{P_n^1(\cos\theta)}{\widehat{H}_n^{(2)\prime}(k_0a)\sin\theta}-\frac{P'(\cos\theta)\sin\theta}{j\widehat{H}_n^{(2)}(k_0a)}\right\}
\end{aligned}
$$

Equation 1 agrees with Equation (6-103) of [2].

$$
\begin{aligned}
H_\phi &= -\frac{1}{r}\frac{\partial A_r^+}{\partial \theta} + \frac{1}{j\omega\mu_0 r\sin\theta}\frac{\partial^2 F_r^+}{\partial r\partial\phi} \\
&= -\frac{E_0}{\omega\mu_0 r}\left[\cos\phi\sum_{n=1}^{\infty}\left[a_n\widehat{J}_n\left(k_0 r\right) + b_n\widehat{H}_n^{(2)}\left(k_0 r\right)\right]\frac{\partial}{\partial\theta}P_n^1\left(\cos\theta\right)\right] \\
&\quad + \frac{E_0}{j\omega\mu_0 k_0 r\sin\theta}\left[\frac{\partial}{\partial\phi}\left(\sin\phi\right)\sum_{n=1}^{\infty}\frac{\partial}{\partial r}\left[a_n\widehat{J}_n\left(k_0 r\right) + c_n\widehat{H}_n^{(2)}\left(k_0 r\right)\right]P_n^1\left(\cos\theta\right)\right] \\
&= \frac{E_0\cos\phi}{\eta_0 k_0 r}\sum_{n=1}^{\infty}\left[a_n\widehat{J}_n\left(k_0 r\right) + b_n\widehat{H}_n^{(2)}\left(k_0 r\right)\right]P_n^{1\prime}\left(\cos\theta\right)\sin\theta - j\left[a_n\widehat{J}_n'\left(k_0 r\right) + c_n\widehat{H}_n^{(2)\prime}\left(k_0 r\right)\right]\frac{P_n^1\left(\cos\theta\right)}{\sin\theta}
\end{aligned}
$$

At $r = a$,

$$
\begin{aligned}
H_\phi &= \frac{E_0\cos\phi}{k_0\eta_0 a}\sum_{n=1}^{\infty}\left[a_n\widehat{J}_n\left(k_0 a\right) - a_n\frac{\widehat{J}_n'\left(k_0 a\right)}{\widehat{H}_n^{(2)\prime}\left(k_0 a\right)}\widehat{H}_n^{(2)}\left(k_0 a\right)\right]P_n^{1\prime}\left(\cos\theta\right)\sin\theta \\
&\quad -j\left[a_n\widehat{J}_n'\left(k_0 a\right) - a_n\frac{\widehat{J}_n\left(k_0 a\right)}{\widehat{H}_n^{(2)}\left(k_0 a\right)}\widehat{H}_n^{(2)\prime}\left(k_0 a\right)\right]\frac{P_n^1\left(\cos\theta\right)}{\sin\theta} \\
&= \frac{E_0\cos\phi}{k_0\eta_0 a}\sum_{n=1}^{\infty}a_n\left\{\begin{array}{c}\left[\widehat{J}_n\left(k_0 a\right)\widehat{H}_n^{(2)\prime}\left(k_0 a\right) - \widehat{J}_n'\left(k_0 a\right)\widehat{H}_n^{(2)}\left(k_0 a\right)\right]\frac{P_n^{1\prime}(\cos\theta)\sin\theta}{\widehat{H}_n^{(2)\prime}(k_0 a)} \\ +j\left[\widehat{J}_n\left(k_0 a\right)\widehat{H}_n^{(2)\prime}\left(k_0 a\right) - \widehat{J}_n'\left(k_0 a\right)\widehat{H}_n^{(2)}\left(k_0 a\right)\right]\frac{P_n^1(\cos\theta)}{\widehat{H}_n^{(2)}(k_0 a)\sin\theta}\end{array}\right\} \\
&= \frac{-j}{\eta_0}E_0\frac{\cos\phi}{k_0 a}\sum_{n=1}^{\infty}a_n\left\{\frac{P_n^{1\prime}\left(\cos\theta\right)\sin\theta}{\widehat{H}_n^{(2)\prime}\left(k_0 a\right)} + \frac{jP_n^1\left(\cos\theta\right)}{\widehat{H}_n^{(2)}\left(k_0 a\right)\sin\theta}\right\}
\end{aligned}
$$

which allows us to calculate the $\widehat{\theta}$ directed electric current density:

$$
\begin{aligned}
\widehat{\theta}J_\theta &= -\widehat{r}\times\widehat{\phi}H_\phi \qquad (2)\\
J_\theta &= \frac{j}{\eta_0}E_0\frac{\cos\phi}{k_0 a}\sum_{n=1}^{\infty}a_n\left\{\frac{P_n^{1\prime}\left(\cos\theta\right)\sin\theta}{\widehat{H}_n^{(2)\prime}\left(k_0 a\right)} + \frac{jP_n^1\left(\cos\theta\right)}{\widehat{H}_n^{(2)}\left(k_0 a\right)\sin\theta}\right\}
\end{aligned}
$$

Equation 2 agrees with Equation 6-103 in [2].

3.2 Summary of the Analytical Solution

3.2.1 Currents

$$
\begin{aligned}
J_\theta &= \frac{j}{\eta_0}E_0\frac{\cos\phi}{k_0 a}\sum_{n=1}^{\infty}a_n\left\{\frac{P_n^{1\prime}\left(\cos\theta\right)\sin\theta}{\widehat{H}_n^{(2)\prime}\left(k_0 a\right)} + \frac{jP_n^1\left(\cos\theta\right)}{\widehat{H}_n^{(2)}\left(k_0 a\right)\sin\theta}\right\} \\
J_\phi &= \frac{j}{\eta_0}E_0\frac{\sin\phi}{k_0 a}\sum_{n=1}^{\infty}a_n\left\{\frac{P_n^1\left(\cos\theta\right)}{\widehat{H}_n^{(2)\prime}\left(k_0 a\right)\sin\theta} - \frac{P'\left(\cos\theta\right)\sin\theta}{j\widehat{H}_n^{(2)}\left(k_0 a\right)}\right\}
\end{aligned}
$$

3.2.2 Near Fields

$$
E_r = -jE_0\cos\phi\sum_{n=1}^{\infty}\left[a_n\widehat{J}_n''\left(k_0 r\right) + b_n\widehat{H}_n^{(2)\prime\prime}\left(k_0 r\right)\right]P_n^1\left(\cos\theta\right) + \left[a_n\widehat{J}_n\left(k_0 r\right) + b_n\widehat{H}_n^{(2)}\left(k_0 r\right)\right]P_n^1\left(\cos\theta\right)
$$

$$E_\theta = \frac{-E_0 \cos\phi}{k_0 r} \sum_{n=1}^{\infty} \left[a_n \widehat{J}_n (k_0 r) + c_n \widehat{H}_n^{(2)} (k_0 r) \right] \frac{P_n^1 (\cos\theta)}{\sin\theta} - j \left[a_n \widehat{J}_n' (k_0 r) + b_n \widehat{H}_n^{(2)\prime} (k_0 r) \right] P_n^{1\prime} (\cos\theta) \sin\theta$$

$$E_\phi = \frac{-E_0 \sin\phi}{k_0 r} \sum_{n=1}^{\infty} \left[a_n \widehat{J}_n (k_0 r) + c_n \widehat{H}_n^{(2)} (k_0 r) \right] P_n^{1\prime} (\cos\theta) \sin\theta - j \left[a_n \widehat{J}_n' (k_0 r) + b_n \widehat{H}_n^{(2)\prime} (k_0 r) \right] \frac{P_n^1 (\cos\theta)}{\sin\theta}$$

$$H_r = \frac{-jE_0}{\eta_0} \sin\phi \sum_{n=1}^{\infty} \left[a_n \widehat{J}_n'' (k_0 r) + c_n \widehat{H}_n^{(2)\prime\prime} (k_0 r) \right] P_n^1 (\cos\theta) + \left[a_n \widehat{J}_n (k_0 r) + c_n \widehat{H}_n^{(2)} (k_0 r) \right] P_n^1 (\cos\theta)$$

$$H_\theta = \frac{-E_0 \sin\phi}{\eta_0 k_0 r} \sum_{n=1}^{\infty} \left[a_n \widehat{J}_n (k_0 r) + b_n \widehat{H}_n^{(2)} (k_0 r) \right] \frac{P_n^1 (\cos\theta)}{\sin\theta} - j \left[a_n \widehat{J}_n' (k_0 r) + c_n \widehat{H}_n^{(2)\prime} (k_0 r) \right] P' (\cos\theta) \sin\theta$$

$$H_\phi = \frac{E_0 \cos\phi}{\eta_0 k_0 r} \sum_{n=1}^{\infty} \left[a_n \widehat{J}_n (k_0 r) + b_n \widehat{H}_n^{(2)} (k_0 r) \right] P_n^{1\prime} (\cos\theta) \sin\theta - j \left[a_n \widehat{J}_n' (k_0 r) + c_n \widehat{H}_n^{(2)\prime} (k_0 r) \right] \frac{P_n^1 (\cos\theta)}{\sin\theta}$$

3.2.3 Far Fields

$$E_\theta^s = \frac{jE_0}{k_0 r} e^{-jk_0 r} \cos\phi \sum_{n=1}^{\infty} j^n \left\{ b_n P_n^{1\prime} (\cos\theta) \sin\theta - c_n \frac{P_n^1 (\cos\theta)}{\sin\theta} \right\}$$

$$E_\phi^s = \frac{jE_0}{k_0 r} e^{-jk_0 r} \sin\phi \sum_{n=1}^{\infty} j^n \left\{ b_n \frac{P_n^1 (\cos\theta)}{\sin\theta} - c_n P_n^{1\prime} (\cos\theta) \sin\theta \right\}$$

3.3 Code Implementation of the Analytical Solution

The formulas in Section 3.2 were implemented in the code **pec_sphere.** **Pec_sphere** calculates quantities of interest versus θ, which varies from 1^0 to 179^0 in 1^0 increments. The other two observation coordinates, ϕ_{obs} and r_{obs}, are set by the user. In the code, $E_0 = 1.0$ V/m.

User input to **pec_sphere** is interactive and consists of the following:

- Number of terms N used in the summations.
- Frequency (Hertz).
- Sphere radius a (meters).
- Observation radius r_{obs} (meters).
- Observation phi ϕ_{obs} (degrees).

The results are written to five output files, each of which contain 179 rows (1 row per θ value) and seven columns. When necessary, zeros are put in certain columns of each row in order to make the format consistent. All angles (θ and phase) are given in degrees.

Output files:

- **pec_sphere_jt.txt**: θ, $|J_\theta|$, phase J_θ, $0.0, 0.0, 0.0, 0.0$
- **pec_sphere_jp.txt**: θ, $|J_\phi|$, phase J_ϕ, $0.0, 0.0, 0.0, 0.0$
- **pec_sphere_enf.txt**: θ, $|E_r|$, phase E_r, $|E_\theta|$, phase E_θ, $|E_\phi|$, phase E_ϕ
- **pec_sphere_hnf.txt**: θ, $|H_r|$, phase H_r, $|H_\theta|$, phase H_θ, $|H_\phi|$, phase H_ϕ
- **pec_sphere_ff.txt**: θ, 0.0, 0.0, $\left| re^{+jkr} E_\theta^{ff} \right|$, phase $re^{+jkr} E_\theta^{ff}$, $\left| re^{+jkr} E_\phi^{ff} \right|$, phase $re^{+jkr} E_\phi^{ff}$.

The first two files (**pec_sphere_jt.txt** and **pec_sphere_jp.txt**) contain the $\widehat{\theta}$ and $\widehat{\phi}$ directed electric current density that exists on the surface of the sphere at ϕ_{obs}. The next two files (**pec_sphere_enf.txt** and **pec_sphere_hnf.txt**) contain the spherical components of total E and H fields in the near field region at (r_{obs}, ϕ_{obs}). The last file (**pec_sphere_ff.txt**) contains the $\widehat{\theta}$ and $\widehat{\phi}$ directed components of E^s in the far field multiplied by the factor $\left(re^{+jk_0r}\right)$.

3.4 Convergence Study of the Analytical Solution

We will first examine the convergence behavior of the analytical solution as we increase the number of terms in the summations. Anticipating that this solution will eventually be compared to a numerical solution, we will use a sphere radius of $a = 0.9989497$ meters for reasons that will be explained later. We will observe all quantities at $\phi_{obs} = 45^0$. Near field quantities will be observed at $r_{obs} = 1.1$ meters. We will look at convergence for three different frequencies: $f = 2.997925 \times 10^7$ Hz ($k_0 a \approx 0.2\pi$), $f = 2.997925 \times 10^8$ Hz ($k_0 a \approx 2.0\pi$), and $f = 2.997925 \times 10^9$ Hz ($k_0 a \approx 20.0\pi$), which span the frequency range of the numerical solutions.

In the following tables we compare the root mean squared relative error (RE_{rms}), which is defined as

$$\mathrm{RE}_{rms} = \sqrt{\frac{1}{179^0}\int_{0.5^0}^{179.5^0} \frac{\left|R_N(\theta) - R_{exact}(\theta)\right|^2}{\left|R_{exact}^{\max}\right|^2} d\theta} \tag{3}$$

where $R_N(\theta)$ is the compared quantity (J_θ, E_ϕ, etc...) summed up to N modes, $R_{exact}(\theta)$ is the exact quantity and $R_{exact}^{\max}$ is the maximum value of $|R_{exact}|$ over all values of θ. This choice of normalization keeps errors in the small values of R_N from dominating RE_{rms}. For the tables in this section we will let $R_{exact} = R_{120}$ and then demonstrate that the answer has converged to eight digits of accuracy (indicated by $\mathrm{RE}_{rms} = 0.0$ in the tables). Each of the table entries gives RE_{rms} as a function of number of terms (N) for various quantities calculated. Note that RE_{rms} is the actual error and not a percentage.

For the low frequency, $f = 2.997925 \times 10^7$ Hz, the analytical solution has converged to eight digits in 20 terms.

N	J_θ	J_ϕ
5	0.263×10^{-2}	0.321×10^{-2}
10	0.280×10^{-8}	0.132×10^{-7}
20	0.0	0.0

N	E_r	E_θ	E_ϕ	E_θ^{ff}	E_ϕ^{ff}
5	0.359×10^{-2}	0.973×10^{-2}	0.793×10^{-2}	0.175×10^{-5}	0.166×10^{-5}
10	0.408×10^{-8}	0.290×10^{-7}	0.206×10^{-7}	0.0	0.0
20	0.0	0.0	0.0	0.0	0.0

N	H_r	H_θ	H_ϕ	Maximum Error
5	0.121×10^{-1}	0.347×10^{-2}	0.284×10^{-2}	0.121×10^{-1}
10	0.169×10^{-7}	0.684×10^{-8}	0.584×10^{-8}	0.290×10^{-7}
20	0.0	0.0	0.0	0.0

For the intermediate frequency, $f = 2.997925 \times 10^8$ Hz, the analytical solution has converged to eight digits in 30 terms.

N	J_θ	J_ϕ
10	0.586×10^{-1}	0.536×10^{-1}
20	0.498×10^{-7}	0.696×10^{-7}
30	0.0	0.0

N	E_r	E_θ	E_ϕ	E_θ^{ff}	E_ϕ^{ff}
10	0.116	0.662×10^{-1}	0.689×10^{-1}	0.218×10^{-2}	0.196×10^{-2}
20	0.263×10^{-6}	0.290×10^{-6}	0.198×10^{-6}	0.0	0.0
30	0.0	0.0	0.0	0.0	0.0

N	H_r	H_θ	H_ϕ	Maximum Error
10	0.145	0.799×10^{-1}	0.830×10^{-1}	0.145
20	0.570×10^{-6}	0.222×10^{-6}	0.144×10^{-6}	0.570×10^{-6}
30	0.0	0.0	0.0	0.0

Finally, for the high frequency, $f = 2.997925 \times 10^9$ Hz, the analytical solution needs 110 terms in order to converge to eight digits.

N	J_θ	J_ϕ
10	0.691	0.475
50	0.483	0.203
70	0.263×10^{-1}	0.143×10^{-1}
90	0.248×10^{-7}	0.350×10^{-7}
100	0.0	0.201×10^{-11}
110	0.0	0.0

N	E_r	E_θ	E_ϕ	E_θ^{ff}	E_ϕ^{ff}
10	0.482	0.386	0.496	0.899×10^{-1}	0.885×10^{-1}.
50	0.458	0.218	0.382	0.384×10^{-1}	0.384×10^{-1}
70	0.202	0.778×10^{-1}	0.148	0.102×10^{-3}	0.915×10^{-4}
90	0.489×10^{-5}	0.322×10^{-5}	0.290×10^{-5}	0.0	0.0
100	0.322×10^{-8}	0.330×10^{-8}	0.180×10^{-8}	0.0	0.0
110	0.0	0.0	0.0	0.0	0.0

N	H_r	H_θ	H_ϕ	Maximum Error
10	0.452	0.397	0.550	0.550
50	0.402	0.178	0.404	0.458
70	0.183	0.608×10^{-1}	0.149	0.202
90	0.457×10^{-5}	0.245×10^{-5}	0.283×10^{-5}	0.489×10^{-5}
100	0.158×10^{-7}	0.305×10^{-8}	0.319×10^{-8}	0.158×10^{-7}
110	0.0	0.0	0.0	0.0

We conclude that if we use 120 terms in the analytical solution, the solution is accurate to 8 digits and is adequate for comparing to a numerical solution.

3.5 Procedures for Checking the Numerical Solution of a PEC Sphere

In this section we outline the procedures that must be followed to compare a numerical solution of the PEC sphere to the analytical solution. We not only have to properly set up the input decks to make the

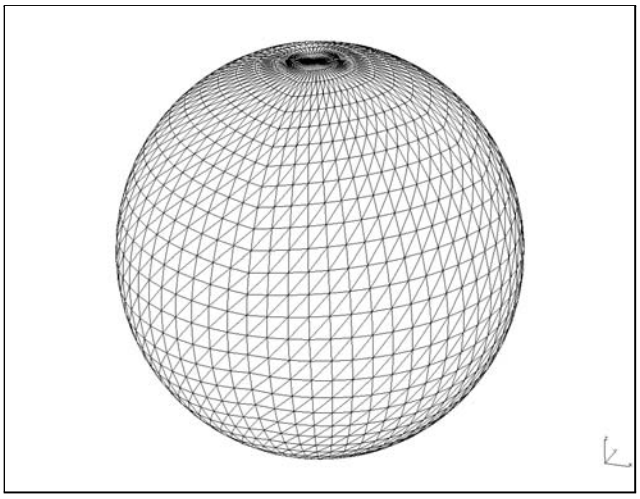

Figure 2. Grid of a sphere using triangular elements with a 10cm edge length

best comparison possible, but also run additional code to get the numerical data in the proper format for comparison.

To organize the many computer runs needed for comparison, we created separate input files for each test problem and named the input and output files to various codes in the comparison sequence consistently. The **sphr_10cm** part of the file name indicates a sphere gridded with elements having a 10 cm edge length. The number/letter combination part of the file name (**0a** for example) indicates the equation to be solved and the excitation. The numbers **0**, **1** and **2** stand for the EFIE, MFIE and CFIE respectively. The letters **a** through **e** indicate different frequencies for the J_θ solution. The letters **f** through **j** indicate different frequencies for the J_ϕ solution. An example file name – **sphr_10cm_0a.eig** – indicates that this problem is a PEC sphere gridded with elements having a 10 cm edge length. The sphere is solved with the EFIE, the frequency is 29.979 MHz, and the excitation is a plane wave with $\theta_{inc} = 180^0, \phi_{inc} = 315^0$ and $H_\phi = (+2.65442 \times 10^{-3}, 0.0)$ (an excitation suitable to obtain J_θ).

3.5.1 Comparing Surface Currents

1. Grid the surface of a sphere with a regular, triangular mesh. Figure 2 shows the mesh used throughout this report, where the radius of the geometric sphere is 1 meter and the element edges are nominally 10 cm long. **Eiger** performs calculations on the faceted element sphere inscribed within the defined geometric sphere so the numerical solution will be for a sphere with a circumference slightly less than that of the geometric sphere. This difference in size must be taken into account for the most precise comparison with analytical results.

The post-processor, **moench,** can calculate the current density along a line located on the surface of the sphere. The current can be either parallel to, or perpendicular to this line. The line is defined by the user listing a set of element pairs. Each pair defines an edge, which is common to both elements. **Moench** calculates the current density flowing across each edge as well as the cumulative distance from edge to edge.

To calculate J_θ we choose pairs of elements whose common edges are perpendicular to $\widehat{\theta}$. The centers of the common edges are all located at $\phi_{obs} = 315^0$ and the edges are chosen in an order so that θ varies from smallest to largest value. The first edge chosen is located an arc distance of 0.0945 meters from the sphere axis. To calculate J_ϕ we choose pairs of elements whose common edges are perpendicular to $\widehat{\phi}$ at $\phi_{obs} = 270^0$. Again, the edges are chosen in an order so that θ varies from smallest to largest value. The

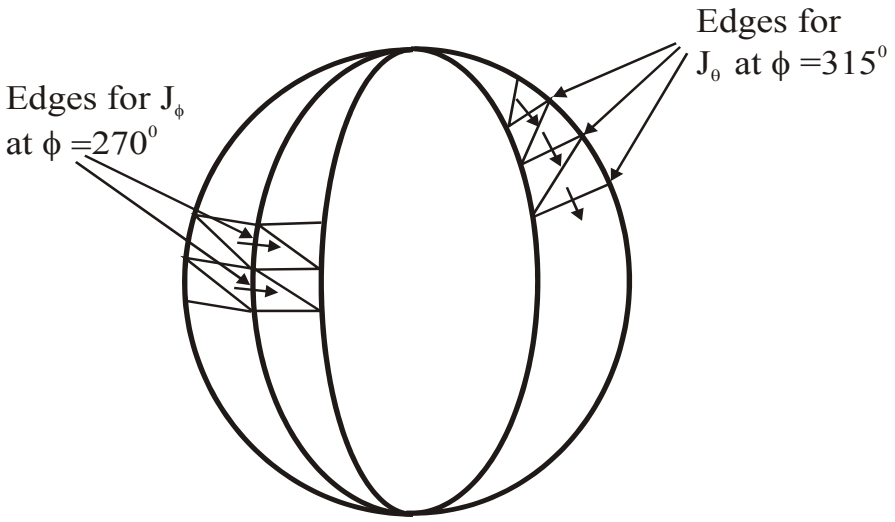

Figure 3. Generating an element list to plot current

center of the first edge is located an arc distance of 0.0523 meters from the sphere axis. Figure 3 shows a few elements from Figure 2 to illustrate these points. Our strategy throughout this report will be to always keep the grid and these element pairs the same and vary frequency and angle of incidence in order to compare to various analytical quantities.

Since we are comparing to physical currents in the analytical solution, we must make the grid so that the element normals point outward in order to avoid sign errors.

2. Run the pre-processor, **jungfrau**, to define the electromagnetic problem. The incident plane wave in the analytical solution propagates in the $+\widehat{z}$ direction. Therefore, we defined the incident plane wave in **jungfrau** to have $\theta_{inc} = 180^0$. We then choose ϕ_{inc} in **jungfrau** to orient the incident wave with respect to the elements chosen in Step 1.

For J_θ we set $\phi_{inc} = 315^0$ and $H_\phi = (+2.65442 \times 10^{-3}, 0.0)$ A/m, which aligns the incident 1 V/m E field with the center of the element edges at $\phi_{obs} = 315^0$ and drives the maximum current across these edges. For the analytical solution we will set $\phi_{obs} = 0^0$ to align the observation angle with the incident E field.

For J_ϕ we set $\phi_{inc} = 0^0$ and $H_\phi = (+2.65442 \times 10^{-3}, 0.0)$ A/m. This drives the maximum J_ϕ across the edges at $\phi_{obs} = 270^0$. For the analytical solution we will also set $\phi_{obs} = 270^0$.

Note that since the edges for J_θ and J_ϕ are not at the same value of ϕ, (and can never be at the same value of ϕ because of discretization) we must create an input file for each comparison and run **eiger** multiple times. An example **jungfrau** input file for J_θ is **sphr_10cm_0a.in**, which is printed in Appendix II.

3. Run **eiger**. Example input is **sphr_10cm_0a.eig**. Example output is **sphr_10cm_0a.mnh.**

4. Run **moench** asking for unknowns along a line (the ul option) and give the set of element pairs from Step 1 to plot either J_θ or J_ϕ along a constant ϕ value. An example **moench** input file for J_θ is **moench_sphr10cm_jt.in,** which is printed in Appendix II. Output is given in a user-named ***.lin1** file (**sphr_10cm_0a.lin1**, for example).

5. Use a text editor to strip the header information from the ***.lin1** file. The zero location of the

***.lin1** file is the element edge designated by the first pair of elements, which is not the zero location of the analytical solution. Run **moench_current_offset** to add the proper location offset to the first column of the *.lin1 file. For J_θ we add 0.0945 meters and for J_ϕ we add 0.0523 meters. An example output file is **jt_10cm0a_offset.txt**. This completes the numerical portion of the comparison.

6. Run **pec_sphere** to obtain the analytic solution. The number of terms (n) is set to be 120 for each run based on what we found in the convergence studies in Section 3.4. The frequency of the analytical solution is identical to that of the numerical solution. The radius of the analytic sphere is slightly smaller than 1.0 meters ($a = 0.9989497$ meters) so that the numerical element sphere and the analytic sphere have the same circumference. To compare with the numerical solution of J_θ, ϕ_{obs} is set to be 0^0 (recall that the analytic E field is aligned along $\phi = 0^0$). To compare with the numerical solution of J_ϕ, ϕ_{obs} is set to be 270^0. The observation radius r_{obs} is not used in calculating the current and can be set to any value. The input file for J_θ (**pec_sphere.in**) is printed in Appendix II. J_θ is output to the file **pec_sphere_jt.txt** and J_ϕ is output to **pec_sphere_jp.txt**.

7. Run **sphere_surface_compare** to find the point-wise relative error and root mean squared relative error (RE_{rms} given by Equation 3) between **pec_sphere_jt.txt** and **jt_10cm0a_offset.txt**. When applying Equation 3 we assume that the analytic solution is the exact solution (R_{exact}) and the numerical solution is R_N. Since **jt_10cm0a_offset.txt** contains non-uniformly spaced data, the code linearly interpolates the analytical solution. Relative error as a function of θ is output in **error.txt**; current as a function of θ is output in **jt_plot.txt**.

3.5.2 Comparing Normal E fields

Eiger can calculate the E field normal to and at the centroid of a set of user-designated elements without resorting to **moench**. The following procedure allows us to compare the numerical E_n to the analytical solution.

1. Step 1 is the same as in comparing surface currents.

2. Run **jungfrau** with the same incident field as was used in calculating J_θ. Request the normal field for the set of elements used for plotting J_θ. These elements have centroids that are clustered around $\phi_{obs} = 315^0$. The elements are ordered so that θ varies from smallest to largest value.

3. Run **eiger**. Example output file containing the normal fields is **sphr_10cm_0a.nor.**

4. Run **eiger_enormal_offset,** which calculates the spherical coordinates of each E_n element's centroid. The coordinates will vary non-uniformly in θ and may vary in ϕ as well, since due to the construction of the grid, the element centroids may not be perfectly aligned along ϕ_{obs}. **Eiger_enormal_offset** rejects elements whose centroids fall outside a user-defined tolerance ($\Delta\phi$) around ϕ_{obs} and outputs E_n on the remaining elements to a user-named file. An example output file is **enormal_10cm0a_offset.txt**. This completes the numerical portion of the comparison.

5. Run **pec_sphere** with $\phi_{obs} = 0.0^0$ and $r_{obs} = 0.9989297$ meters (the sphere radius). Output is **pec_sphere_enf.txt.**

6. Run **sphere_surface_compare**. Relative error as a function of θ is output in **error.txt**; E_n as a function of θ is output in **jt_plot.txt**. Only the first two columns in each file are used.

3.5.3 Comparing Near Fields

In this section we will only consider the E near field comparison since the H near field is analogous.

1-3. Steps 1 through 3 are the same as those for comparing the J_θ surface current.

4. Run **sphere_jfg_build** to generate a grid of bars along an arc. The bars will define points where near fields are to be calculated. The code generates 179 disconnected bar elements all having centers at user-defined coordinates r_{arc} and ϕ_{arc}. The θ_{arc} coordinates range from 1^0 to 179^0 in 1^0 increments. The points and elements are written out in ***.jfg** format. This special grid allows us to exactly match the observation points of the analytic case, eliminating the need for interpolation, which was necessary in comparing surface quantities like current and normal E field. For this test case we generated an arc at $r_{arc} = 1.1$ meters and $\phi_{arc} = 0^0$. Note that since the input E field is directed along $\phi_{inc} = 315^0$ we are observing the near fields at an angle $+45^0$ with respect to the incident E field. We need to account for this when running the analytic case.

5. Run **moench** asking for near fields (nf option) on a read-in grid (re option) and give the name of the ***.jfg** file generated in Step 4 as the read-in grid. An example input file **moench_sphr1.1_nfld.in** is printed in Appendix II. An example output file is **sphr10cm0a_r1.1_0deg.nfld0**, the name of which indicates that the near field was calculated at a radius of 1.1 meters and $\phi_{obs} = 0^0$.

6. Run **moench_r2s_nfld** to convert the total E and H fields in **sphr10cm0a_r1.1_0deg.nfld0** from rectangular to spherical coordinates. The output is given in two user-named files: one for E fields and the other for H fields. Both files have a format identical to that of the analytic near field file. An example output file for the E field is named **enf_10cm0a.txt.** This completes the numerical portion of the comparison.

7. Run **pec_sphere** with $\phi_{obs} = 45^0$ and $r_{obs} = 1.1$ meters to match the numerical case. An example input file is printed in Appendix II. Output is in **pec_sphere_enf.txt.**

8. Run **sphere_field_compare** to find the relative error as a function of θ and RMS error between near field components. Output is in **error.txt.**

3.5.4 Comparing Far Fields

1-3. Steps 1 through 3 are the same as those for comparing the J_θ surface current.

4. Run **moench** asking for far fields (ff option). Ask for the far fields at a single value of $\phi = 0^0$ and 179 values of θ from 1^0 to 179^0. An example input file **moench_sphr10cm_ffld.in** is printed in Appendix II. An example output file is named **sphr10cm0a_0deg.ffld0**, which indicates that the far field was calculated at $\phi = 0^0$.

5. Run **moench_ffld** to strip out the scattered far field data. An example output file is named **sphr10cm0a_ff.txt**. This completes the numerical portion of the comparison.

6. Run **pec_sphere** with $\phi_{obs} = 45^0$ to match the numerical case. The quantity r_{obs} is unimportant since the observation radius is normalized out of the far field calculation. Output is in **pec_sphere_ff.txt.**

7. Run **sphere_field_compare** to find the relative error as a function of θ and RMS error between far field components. Output is in **error txt.**

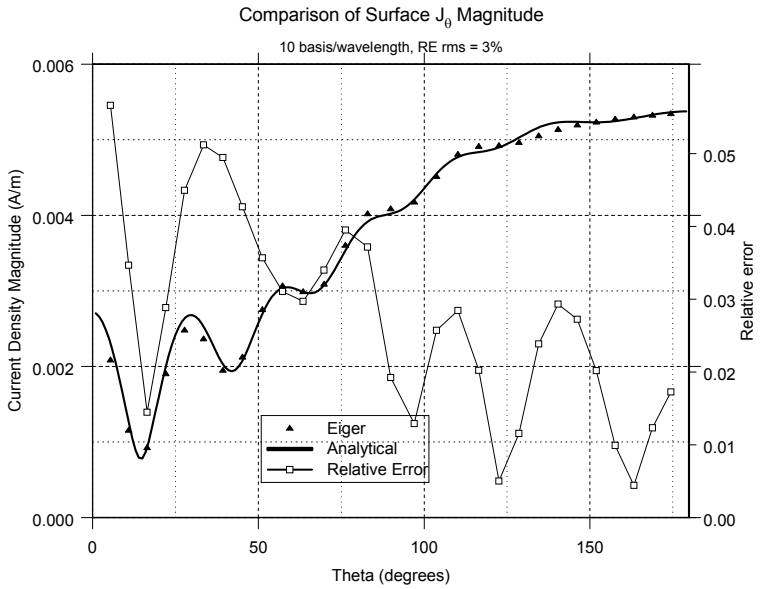

Figure 4. Comparison (left axis) and relative error (right axis) of $|J_\theta|$ vs. θ for $f = 299.7925$ MHz

3.6 Numerical Results

In this section we compare the numerical solution to analytical solution for all quantities of interest, which are the surface current density, all components of E and H in the near field, and E_θ and E_ϕ in the far field. We make the comparison for each of the equations that can be used by **Eiger**: the electric field integral equation (EFIE), the magnetic field integral equation (MFIE) and the combined field integral equation (CFIE). For the EFIE calculation we show plots of all the quantities of interest at a single frequency and summarize the RMS relative error for all frequencies in tables. For the other equations we only show results for the surface current density – showing plots for a single frequency – and summarizing the RMS relative error for all frequencies in tables. Results are also shown for all equations when the frequency is such that an internal resonance occurs.

3.6.1 EFIE

In Figures 4 through 14 we show results for the EFIE calculation. In each figure we compare the magnitude of each quantity of interest computed by **Eiger** (isolated solid triangles) to the quantity calculated analytically (solid lines) as a function of θ. The left hand axis is the magnitude of the quantity. Also plotted in each figure is the relative error (line with open squares), which goes with the right hand axis. The frequency was set at 299.7925 MHz, which corresponds to the rule of thumb that the element edge length should be approximately 1/10 of a wave-length or smaller for good results. The relative error measures both magnitude and phase. Therefore, a high relative error when the magnitude shows good comparison implies that differences in phase are dominating the error. The RE_{rms} (Equation 3) is evaluated and printed in the subtitle.

In the tables below we study the RMS relative error for all quantities as we vary the frequency, keeping the grid fixed. Column 1 is the frequency in MHz, column 2 is the number of basis functions per wavelength, and the remaining columns shows the RMS relative error for each quantity. The last

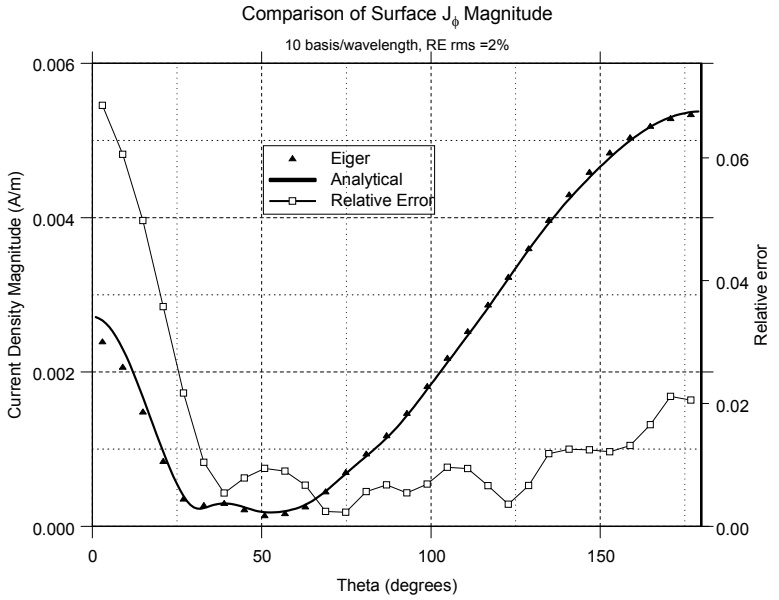

Figure 5. Comparison (left axis) and relative error (right axis) of $|J_\phi|$ vs. θ for $f = 299.7925$ MHz

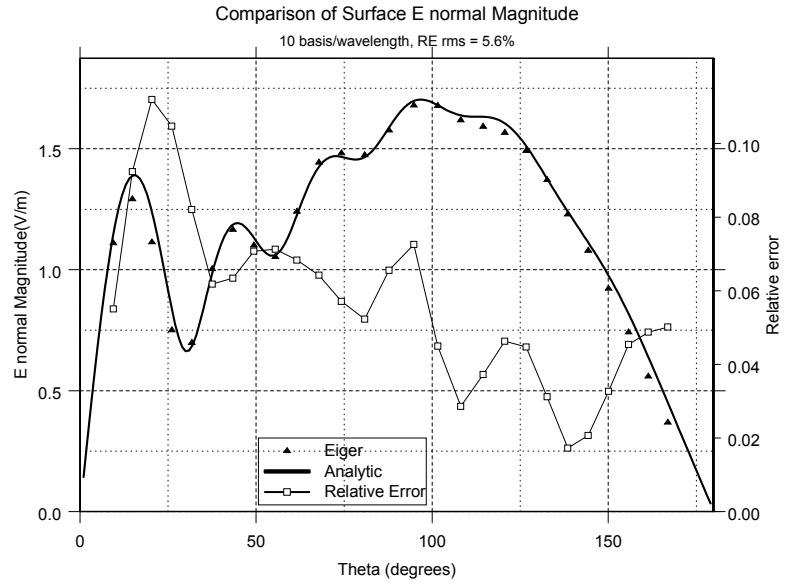

Figure 6. Comparison (left axis) and relative error (right axis) of E_n vs. θ for $f = 299.7925$ MHz

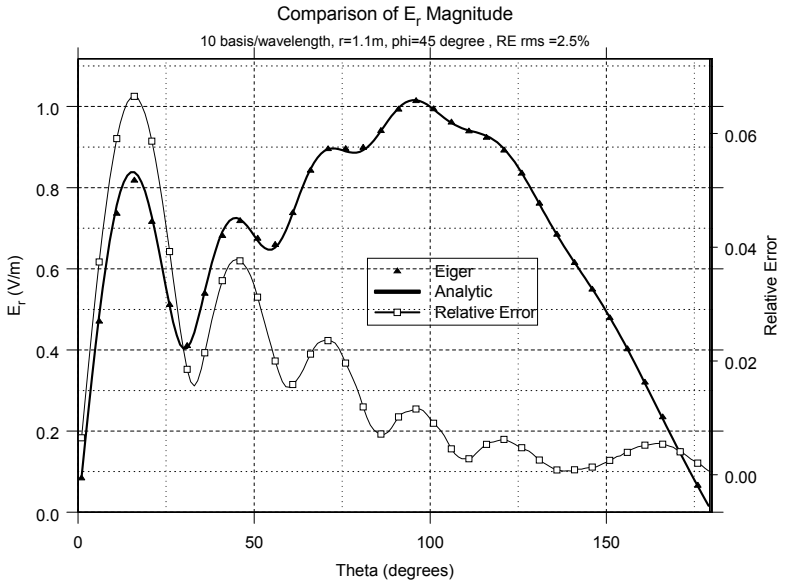

Figure 7. Comparison (left axis) and relative error (right axis) of E_r vs. θ for $f = 299.7925$ MHz

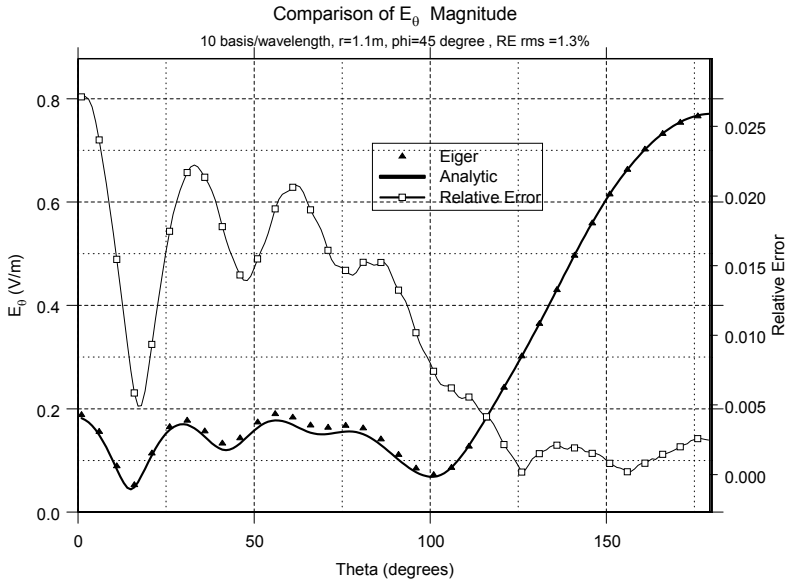

Figure 8. Comparison (left axis) and relative error (right axis) of E_θ vs. θ for $f = 299.7925$ MHz

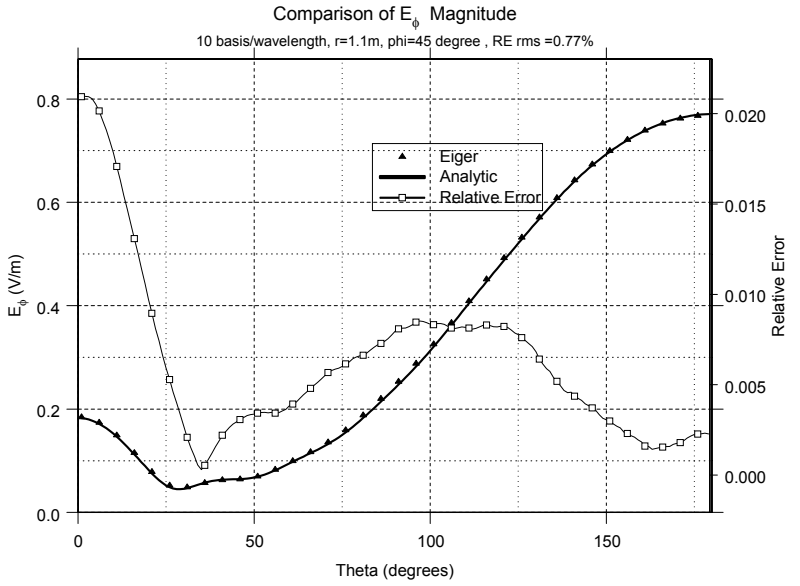

Figure 9. Comparison (left axis) and relative error (right axis) of E_ϕ vs. θ for $f = 299.7925$ MHz

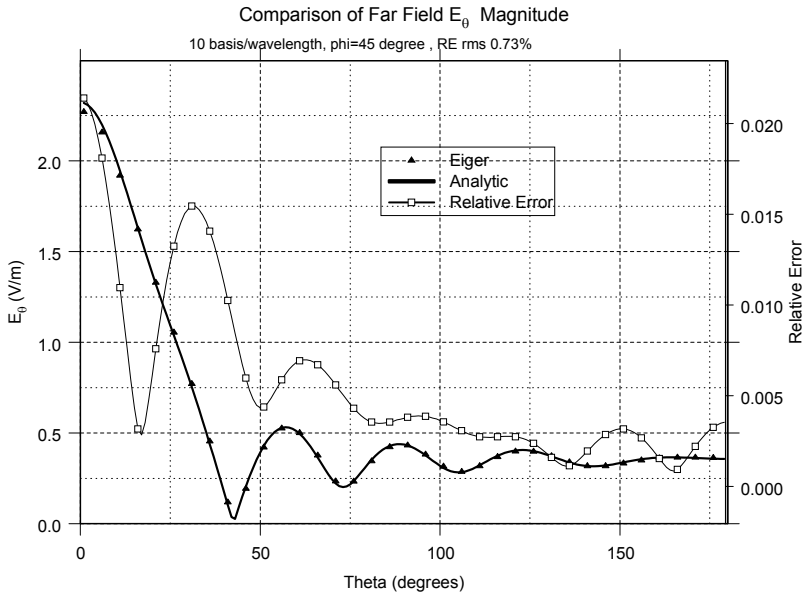

Figure 10. Comparison (left axis) and relative error (right axis) of E_θ^{ff} vs. θ for $f = 299.7925$ MHz

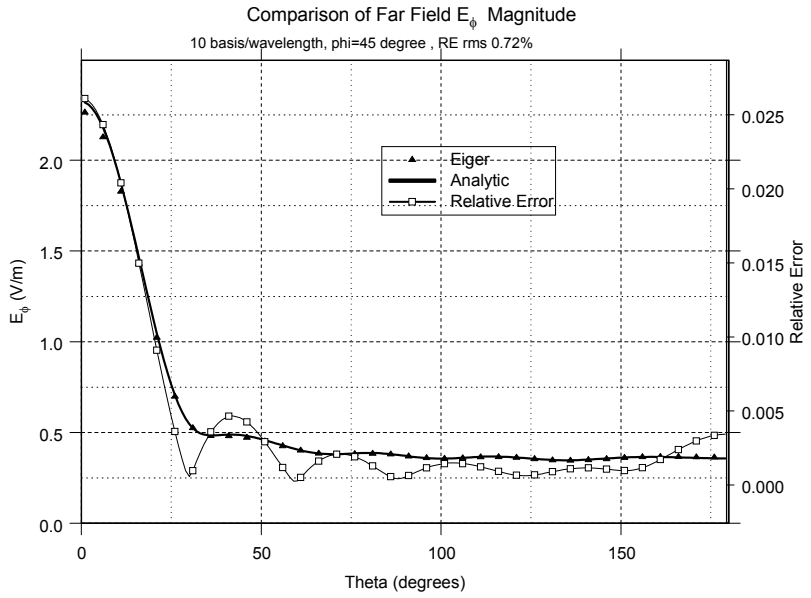

Figure 11. Comparison (left axis) and relative error (right axis) of E_ϕ^{ff} vs. θ for $f = 299.7925$ MHz

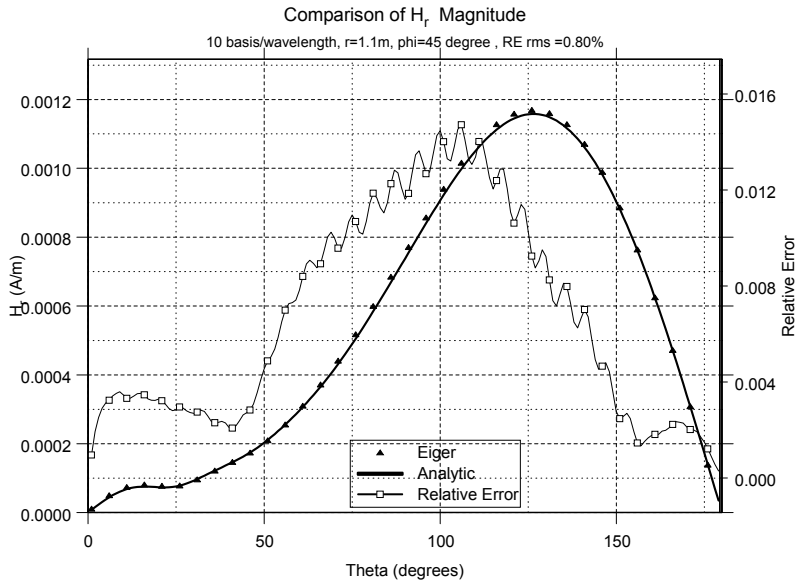

Figure 12. Comparison (left axis) and relative error (right axis) of H_r vs. θ for $f = 299.7925$ MHz

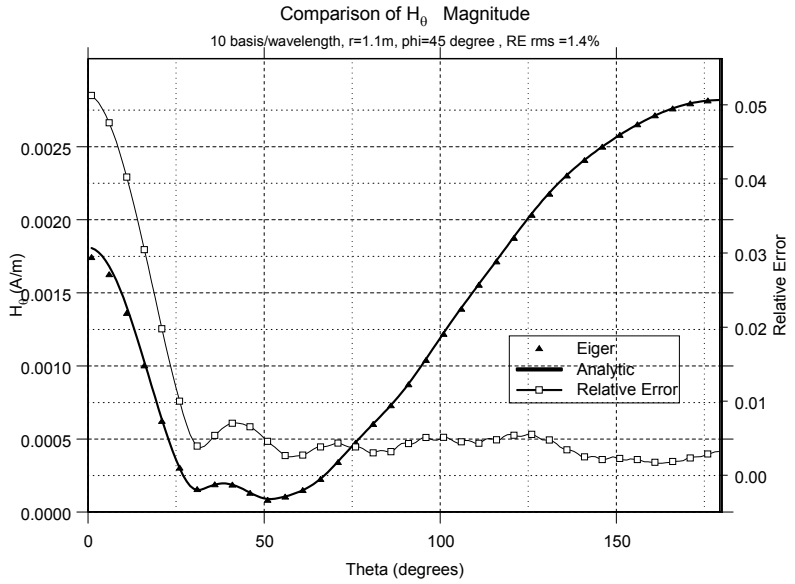

Figure 13. Comparison (left axis) and relative error (right axis) of H_θ vs. θ for $f = 299.7925$ MHz

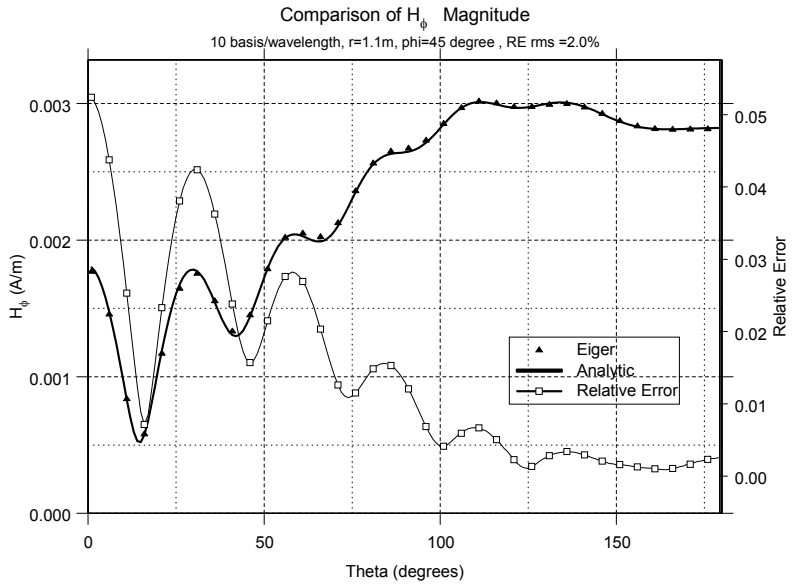

Figure 14. Comparison (left axis) and relative error (right axis) of H_ϕ vs. θ for $f = 299.7925$ MHz

column of the last table shows the maximum error over all the columns. The, maximum relative error increases from 0.77% when we discretize at 100 basis functions per wavelength to 37% when we discretize at 5 basis functions per wavelength. The error increases monotonically as the number of basis functions per wavelength decreases. Also note that the maximum error is usually from the E_n column.

Frequency (MHz)	basis/λ	J_θ	J_ϕ	E_n
29.979	100	0.77×10^{-3}	0.12×10^{-2}	0.51×10^{-2}
199.862	15	0.11×10^{-1}	0.77×10^{-2}	0.25×10^{-1}
299.793	10	0.30×10^{-1}	0.21×10^{-1}	0.56×10^{-1}
428.275	7	0.83×10^{-1}	0.28×10^{-1}	0.10
599.585	5	0.29	0.20	0.37

Frequency (MHz)	basis/λ	E_r	E_θ	E_ϕ	E_θ^{ff}	E_ϕ^{ff}
29.979	100	0.14×10^{-2}	0.77×10^{-2}	0.67×10^{-2}	0.18×10^{-2}	0.24×10^{-2}
199.862	15	0.11×10^{-1}	0.86×10^{-2}	0.58×10^{-2}	0.43×10^{-2}	0.41×10^{-2}
299.793	10	0.25×10^{-1}	0.13×10^{-1}	0.77×10^{-2}	0.73×10^{-2}	0.72×10^{-2}
428.275	7	0.52×10^{-1}	0.20×10^{-1}	0.11×10^{-1}	0.13×10^{-1}	0.12×10^{-1}
599.585	5	0.10	0.35×10^{-1}	0.22×10^{-1}	0.19×10^{-1}	0.18×10^{-1}

Frequency (MHz)	basis/λ	H_r	H_θ	H_ϕ	Max Error
29.979	100	0.55×10^{-2}	0.10×10^{-2}	0.74×10^{-3}	0.77×10^{-2}
199.862	15	0.61×10^{-2}	0.58×10^{-2}	0.77×10^{-2}	0.25×10^{-1}
299.793	10	0.80×10^{-2}	0.14×10^{-1}	0.20×10^{-1}	0.56×10^{-1}
428.275	7	0.11×10^{-1}	0.35×10^{-1}	0.44×10^{-1}	0.10
599.585	5	0.19×10^{-1}	0.95×10^{-1}	0.93×10^{-1}	0.37

3.6.2 MFIE

In Figures 15 through 18 we show results for $|J_\theta|$ and $|J_\phi|$ solved by all three equations that can be applied to the PEC sphere (EFIE, MFIE, and CFIE) compared to the analytic solution. The discretization is 10 basis functions per wavelength. At this frequency, the CFIE shows the best comparison, followed by the EFIE and finally the MFIE.

The following table shows the RMS error for J_θ and J_ϕ at various frequencies when the MFIE is applied.

Frequency (MHz)	basis/λ	J_θ	J_ϕ
29.979	100	0.12×10^{-1}	0.13×10^{-1}
199.862	15	0.24×10^{-1}	0.19×10^{-1}
299.793	10	0.41×10^{-1}	0.32×10^{-1}
428.275	7	0.62×10^{-1}	0.32×10^{-1}
599.585	5	0.11	0.14

3.6.3 CFIE

The following table shows the RMS error for J_θ and J_ϕ at various frequencies when the CFIE is applied. Note that the CFIE has a lower RMS relative error that either the EFIE or MFIE.

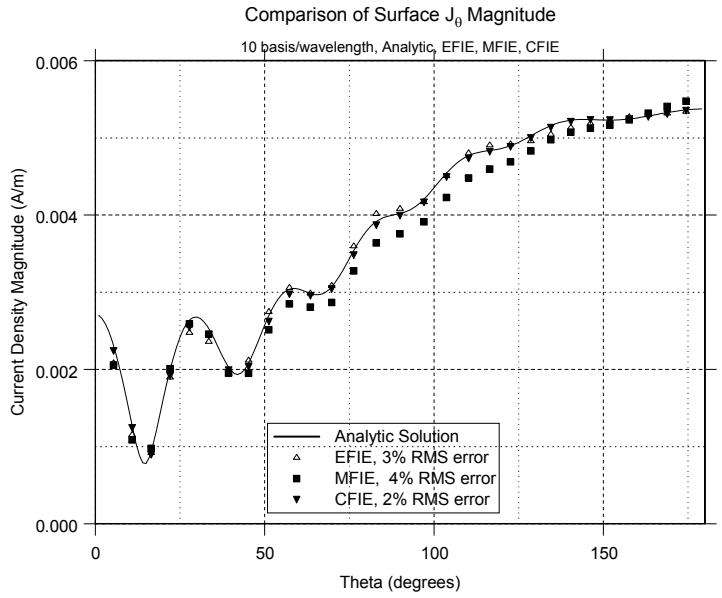

Figure 15. Comparison of $|J_\theta|$ vs. θ as solved by different equations for $f = 299.7925$ MHz

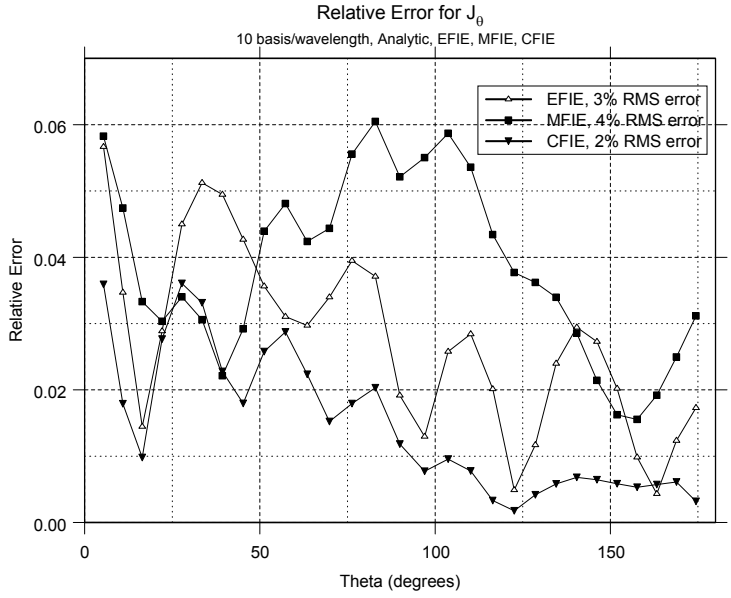

Figure 16. Relative error of J_θ vs. θ as solved by different equations for $f = 299.7925$ MHz

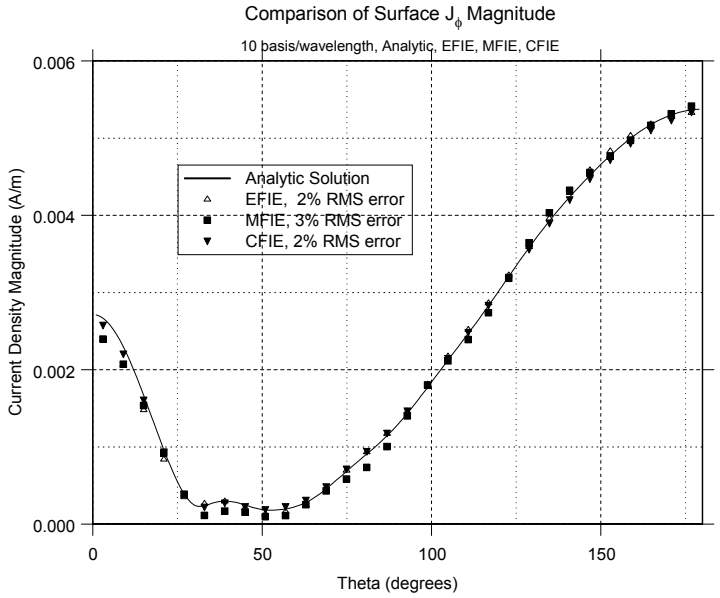

Figure 17. Comparison of $|J_\phi|$ vs. θ as solved by different equations for $f = 299.7925$ MHz

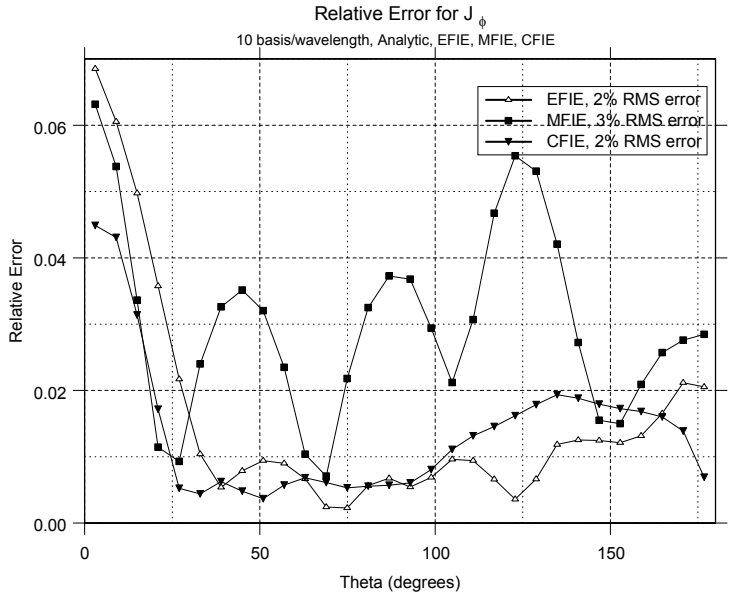

Figure 18. Relative error of J_ϕ vs. θ as solved by different equations for $f = 299.7925$ MHz

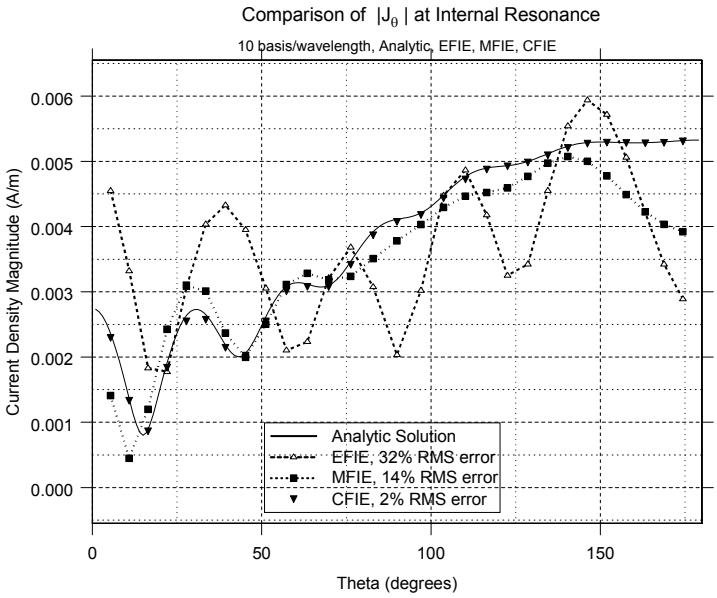

Figure 19. Comparison of $|J_\theta|$ vs. θ as solved by different equations at resonance ($f = 289.70$ MHz)

Frequency (MHz)	basis/λ	J_θ	J_ϕ
29.979	100	0.63×10^{-2}	0.75×10^{-2}
199.862	15	0.98×10^{-2}	0.11×10^{-1}
299.793	10	0.18×10^{-1}	0.16×10^{-1}
428.275	7	0.35×10^{-1}	0.23×10^{-1}
599.585	5	0.67×10^{-1}	0.34×10^{-1}

3.6.4 Internal Resonance Test Case

At certain frequencies, even though we are actually solving a scattering problem, the interior of the surface that defines the sphere becomes resonant causing problems for the EFIE and MFIE formulation. These problems manifest themselves in an impedance matrix with a high condition number and a current density corrupted by the sourceless solution of the resonant cavity. One such frequency for the PEC sphere considered here is 289.70 MHz, ($ka = 6.062$). At this frequency the TM to $\widehat{r}$, n=1, m=4 mode is resonant.

Figure 19 shows $|J_\theta|$ versus θ at the 289.70 MHz as calculated by the EFIE, MFIE and CFIE. Note that only the CFIE maintains its low RMS relative error, as shown in Figure 20. The error for the other two equations increases significantly.

4 Lossless Dielectric Sphere Test Case

4.1 Derivation of the Analytical Solution

If the sphere is a dielectric, with permittivity $\varepsilon_d = \varepsilon_r\varepsilon_0$ and permeability $\mu_d = \mu_r\mu_0$, the potentials

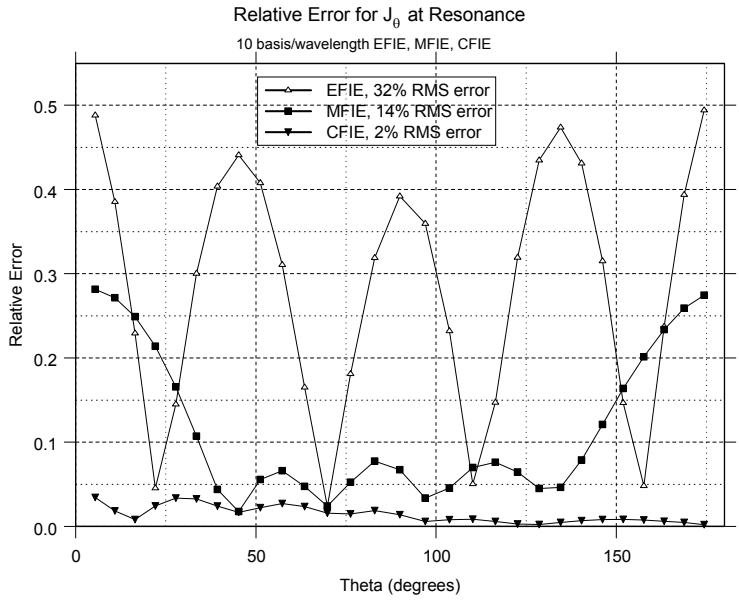

Figure 20. Relative error for J_θ vs. θ as solved by different equations at resonance ($f = 289.70$ MHz)

outside the sphere are given as [2]

$$A_r^+ = \frac{E_0}{\omega\mu_0}\cos\phi\sum_{n=1}^{\infty}\left[a_n\widehat{J}_n\left(k_0r\right)+b_n\widehat{H}_n^{(2)}\left(k_0r\right)\right]P_n^1\left(\cos\theta\right)$$

$$F_r^+ = \frac{E_0}{k_0}\sin\phi\sum_{n=1}^{\infty}\left[a_n\widehat{J}_n\left(k_0r\right)+c_n\widehat{H}_n^{(2)}\left(k_0r\right)\right]P_n^1\left(\cos\theta\right)$$

while the potentials inside the sphere are given as

$$A_r^- = \frac{E_0}{\omega\mu_0}\cos\phi\sum_{n=1}^{\infty}d_n\widehat{J}_n\left(k_dr\right)P_n^1\left(\cos\theta\right)$$

$$F_r^- = \frac{E_0}{k_0}\sin\phi\sum_{n=1}^{\infty}e_n\widehat{J}_n\left(k_dr\right)P_n^1\left(\cos\theta\right)$$

where $k_d=\omega\sqrt{\varepsilon_d\mu_d}$ is the wavenumber in the dielectric material,

$$a_n = \frac{j^{-n}\left(2n+1\right)}{n\left(n+1\right)}$$

$$b_n = \frac{-\sqrt{\varepsilon_d\mu_0}\widehat{J}_n'\left(k_0a\right)\widehat{J}_n\left(k_da\right)+\sqrt{\varepsilon_0\mu_d}\widehat{J}_n\left(k_0a\right)\widehat{J}_n'\left(k_da\right)}{\sqrt{\varepsilon_d\mu_0}\widehat{H}_n^{(2)\prime}\left(k_0a\right)\widehat{J}_n\left(k_da\right)-\sqrt{\varepsilon_0\mu_d}\widehat{H}_n^{(2)}\left(k_0a\right)\widehat{J}_n'\left(k_da\right)}a_n$$

$$c_n = \frac{-\sqrt{\varepsilon_d\mu_0}\widehat{J}_n\left(k_0a\right)\widehat{J}_n'\left(k_da\right)+\sqrt{\varepsilon_0\mu_d}\widehat{J}_n'\left(k_0a\right)\widehat{J}_n\left(k_da\right)}{\sqrt{\varepsilon_d\mu_0}\widehat{H}_n^{(2)}\left(k_0a\right)\widehat{J}_n'\left(k_da\right)-\sqrt{\varepsilon_0\mu_d}\widehat{H}_n^{(2)\prime}\left(k_0a\right)\widehat{J}_n\left(k_da\right)}a_n$$

$$d_n = \frac{-j\sqrt{\varepsilon_d\mu_0}}{\sqrt{\varepsilon_d\mu_0}\widehat{H}_n^{(2)\prime}\left(k_0a\right)\widehat{J}_n\left(k_da\right)-\sqrt{\varepsilon_0\mu_d}\widehat{H}_n^{(2)}\left(k_0a\right)\widehat{J}_n'\left(k_da\right)}a_n$$

$$e_n = \frac{j\sqrt{\varepsilon_0\mu_d}}{\sqrt{\varepsilon_d\mu_0}\widehat{H}_n^{(2)}\left(k_0a\right)\widehat{J}_n'\left(k_da\right)-\sqrt{\varepsilon_0\mu_d}\widehat{H}_n^{(2)\prime}\left(k_0a\right)\widehat{J}_n\left(k_da\right)}a_n$$

Outside the sphere, the fields are the same as given in Section 3.2 with new values of b_n and c_n. Inside the sphere the fields are:

$$\begin{aligned}E_r &= \frac{1}{j\omega\varepsilon_d}\left(\frac{\partial^2}{\partial r^2}+k_d^2\right)A_r^-\\ &= -jE_0\mu_r\cos\phi\sum_{n=1}^{\infty}d_n\left[\widehat{J}_n''\left(k_dr\right)+\widehat{J}_n\left(k_dr\right)\right]P_n^1\left(\cos\theta\right)\end{aligned}$$

$$\begin{aligned}E_\theta &= \frac{-1}{r\sin\theta}\frac{\partial F_r^-}{\partial\phi}+\frac{1}{j\omega\varepsilon_d r}\frac{\partial^2A_r^-}{\partial r\partial\theta}\\ &= \frac{-E_0\cos\phi}{k_0r}\sum_{n=1}^{\infty}\left[e_n\widehat{J}_n\left(k_dr\right)\frac{P_n^1\left(\cos\theta\right)}{\sin\theta}-j\sqrt{\frac{\mu_r}{\varepsilon_r}}d_n\widehat{J}_n'\left(k_dr\right)P_n^{1\prime}\left(\cos\theta\right)\sin\theta\right]\end{aligned}$$

$$\begin{aligned}E_\phi &= \frac{1}{r}\frac{\partial F_r^-}{\partial\theta}+\frac{1}{j\omega\varepsilon_d r\sin\theta}\frac{\partial^2A_r^-}{\partial r\partial\phi}\\ &= \frac{-E_0\sin\phi}{k_0r}\sum_{n=1}^{\infty}\left[e_n\widehat{J}_n\left(k_dr\right)P_n^{1\prime}\left(\cos\theta\right)\sin\theta-j\sqrt{\frac{\mu_r}{\varepsilon_r}}d_n\widehat{J}_n'\left(k_dr\right)\frac{P_n^1\left(\cos\theta\right)}{\sin\theta}\right]\end{aligned}$$

$$\begin{aligned}H_r &= \frac{1}{j\omega\mu_d}\left(\frac{\partial^2}{\partial r^2}+k_d^2\right)F_r^-\\ &= \frac{-jE_0}{\eta_0}\varepsilon_r\sin\phi\sum_{n=1}^{\infty}e_n\left[\widehat{J}_n''\left(k_dr\right)+\widehat{J}_n\left(k_dr\right)\right]P_n^1\left(\cos\theta\right)\end{aligned}$$

$$
\begin{aligned}
H_\theta &= \frac{1}{r\sin\theta}\frac{\partial A_r^-}{\partial\phi} + \frac{1}{j\omega\mu_d r}\frac{\partial^2 F_r^-}{\partial r\partial\theta} \\
&= \frac{-E_0\sin\phi}{\eta_0 k_0 r}\sum_{n=1}^{\infty}\left[d_n\widehat{J}_n\left(k_d r\right)\frac{P_n^1\left(\cos\theta\right)}{\sin\theta} - j\sqrt{\frac{\varepsilon_r}{\mu_r}}e_n\widehat{J}_n'\left(k_d r\right)P_n^{1'}\left(\cos\theta\right)\sin\theta\right] \\
H_\phi &= -\frac{1}{r}\frac{\partial A_r^-}{\partial\theta} + \frac{1}{j\omega\mu_d r\sin\theta}\frac{\partial^2 F_r^-}{\partial r\partial\phi} \\
&= \frac{E_0\cos\phi}{\eta_0 k_0 r}\sum_{n=1}^{\infty}\left[d_n\widehat{J}_n\left(k_d r\right)P_n^{1'}\left(\cos\theta\right)\sin\theta - j\sqrt{\frac{\varepsilon_r}{\mu_r}}e_n\widehat{J}_n'\left(k_d r\right)\frac{P_n^1\left(\cos\theta\right)}{\sin\theta}\right]
\end{aligned}
$$

4.2 Code Implementation of the Analytical Solution

The formulas in Section 4 were implemented in the code **diel_sphere.** **Diel_sphere** calculates quantities of interest versus θ, which varies from 1^0 to 179^0 in 1^0 increments. The other two observation coordinates, ϕ_{obs} and r_{obs}, are set by the user. In the code, $E_0 = 1.0$ V/m. Note that the relative permittivity and permeability (ε_r and μ_r) are both real quantities for the lossless dielectric.

User input to **diel_sphere** is interactive and consists of the following:

- Number of terms used in the summations.
- Frequency (Hertz).
- Relative permittivity of dielectric ε_r (unitless).
- Relative permeability of dielectric μ_r (unitless).
- Sphere radius a (meters).
- Observation radius r_{obs} (meters).
- Observation phi ϕ_{obs} (degrees).

The results are written to seven output files, each of which contain 179 rows (1 row per θ value) and seven columns. When necessary, zeros are put in certain columns of each row in order to make the format consistent. All angles, θ and phase, are given in degrees.

Output files:

- **diel_sphere_jt.txt**: θ, $|J_\theta|$, phase J_θ, $0.0, 0.0, 0.0, 0.0$
- **diel_sphere_jp.txt**: θ, $|J_\phi|$, phase J_ϕ, $0.0, 0.0, 0.0, 0.0$
- **diel_sphere_mt.txt**: θ, $|M_\theta|$, phase M_θ, $0.0, 0.0, 0.0, 0.0$
- **diel_sphere_mp.txt**: θ, $|M_\phi|$, phase M_ϕ, $0.0, 0.0, 0.0, 0.0$
- **diel_sphere_enf.txt**: θ, $|E_r|$, phase E_r, $|E_\theta|$, phase E_θ, $|E_\phi|$, phase E_ϕ
- **diel_sphere_hnf.txt**: θ, $|H_r|$, phase H_r, $|H_\theta|$, phase H_θ, $|H_\phi|$, phase H_ϕ
- **diel_sphere_ff.txt**: θ, $0.0, 0.0$, $\left|re^{+jkr}E_\theta^{ff}\right|$, phase $re^{+jkr}E_\theta^{ff}$, $\left|re^{+jkr}E_\phi^{ff}\right|$, phase $re^{+jkr}E_\phi^{ff}$

The first two files (**diel_sphere_jt.txt** and **diel_sphere_jp.txt**) contain the $\widehat{\theta}$ and $\widehat{\phi}$

directed components of electric current density. The next two files (**diel_sphere_mt.txt** and **diel_sphere_mp.txt**) contain the $\widehat{\theta}$ and $\widehat{\phi}$ directed components of magnetic current density. Unlike the PEC case, which specializes the radius to the surface of the sphere to obtain the current, these results are for $r = r_{obs}$ (not necessarily specialized to the sphere surface). $\overrightarrow{J} = \widehat{r} \times \overrightarrow{H}$ and $\overrightarrow{M} = E \times \widehat{r}$. Therefore, when comparing current density, r_{obs} must be set to be equal to the sphere radius. The next two files (**diel_sphere_enf.txt** and **diel_sphere_hnf.txt**) contain the spherical components of total E and H fields in the near field region at (r_{obs}, ϕ_{obs}). The last file (**diel_sphere_ff.txt**) contains the $\widehat{\theta}$ and $\widehat{\phi}$ directed components of E^s in the far field multiplied by the factor $\left(re^{+jk_0r}\right)$.

4.3 Convergence Study of the Analytical Solution

We will examine the convergence behavior of the analytical solution as we increase the number of terms like we did for the PEC sphere. We will again use a sphere radius of $a = 0.9989497$ meters. Unlike the PEC sphere, we will observe near field quantities just off the surface of the sphere at $r_{obs} = 1.0$ meters and $\phi_{obs} = 45^0$ in order to capture the convergence behavior of the surface currents, which are related to the θ and ϕ components of field at this location. We will look at convergence for the same frequencies as the PEC case: $f = 2.997925 \times 10^7$ Hz, $f = 2.997925 \times 10^8$ Hz, and $f = 2.997925 \times 10^9$ Hz and we will set $\varepsilon_r = 3$, and $\mu_r = 2$.

For the following tables we will again use Equation 3, let $R_{exact} = R_{120}$ and demonstrate that the answer has converged to eight digits of accuracy (indicated by $\text{RE}_{rms} = 0.0$ in the tables). Each of the table entries gives RE_{rms} as a function of number of terms (N) for various quantities calculated. Note that RE_{rms} is the actual error and not a percentage.

For the low frequency, $f = 2.997925 \times 10^7$ Hz, the analytical solution has converged to eight digits in 20 terms.

N	E_r	E_θ	E_ϕ	E_θ^{ff}	E_ϕ^{ff}
5	0.282×10^{-2}	0.238×10^{-2}	0.204×10^{-2}	0.139×10^{-5}	0.128×10^{-5}
10	0.535×10^{-8}	0.926×10^{-8}	0.226×10^{-8}	0.0	0.0
20	0.0	0.0	0.0	0.0	0.0

N	H_r	H_θ	H_ϕ	Maximum Error
5	0.296×10^{-2}	0.256×10^{-2}	0.216×10^{-2}	0.296×10^{-2}
10	0.472×10^{-8}	0.506×10^{-8}	0.751×10^{-8}	0.926×10^{-8}
20	0.0	0.0	0.0	0.0

For the intermediate frequency, $f = 2.997925 \times 10^8$ Hz, the analytical solution has converged to eight digits in 30 terms.

N	E_r	E_θ	E_ϕ	E_θ^{ff}	E_ϕ^{ff}
10	0.573×10^{-1}	0.113	0.132	0.109×10^{-2}	0.164×10^{-2}
20	0.660×10^{-7}	0.178×10^{-7}	0.167×10^{-7}	0.0	0.0
30	0.0	0.0	0.0	0.0	0.0

N	H_r	H_θ	H_ϕ	Maximum Error
10	0.233	0.142	0.908×10^{-1}	0.233
20	0.319×10^{-7}	0.110×10^{-7}	0.203×10^{-7}	0.660×10^{-7}
30	0.0	0.0	0.0	0.0

Finally, for the high frequency, $f = 2.997925 \times 10^9$ Hz, the analytical solution needs 110 terms in order to converge to eight digits.

N	E_r	E_θ	E_ϕ	E_θ^{ff}	E_ϕ^{ff}
10	0.229	0.233	0.231	0.895×10^{-1}	0.900×10^{-1}
50	0.217	0.128	0.150	0.400×10^{-1}	0.395×10^{-1}
70	0.146×10^{-1}	0.797×10^{-2}	0.113×10^{-1}	0.109×10^{-3}	0.125×10^{-3}
90	0.126×10^{-7}	0.667×10^{-8}	0.101×10^{-7}	0.0	0.0
100	0.0	0.0	0.0	0.0	0.0
110	0.0	0.0	0.0	0.0	0.0

N	H_r	H_θ	H_ϕ	Maximum Error
10	0.324	0.181	0.257	0.324
50	0.291	0.102	0.184	0.291
70	0.236×10^{-1}	0.522×10^{-2}	0.110×10^{-1}	0.236×10^{-1}
90	0.185×10^{-8}	0.935×10^{-8}	0.971×10^{-8}	0.126×10^{-7}
100	0.338×10^{-10}	0.0	0.0	0.338×10^{-10}
110	0.0	0.0	0.0	0.0

4.4 Procedures for Checking the Numerical Solution of a Dielectric Sphere

In this section we outline the procedures that must be followed to compare a numerical solution of the dielectric sphere to the analytical solution. All of the files are tagged with the name **sphr_10cm** and a number/letter combination. The number part (**3**) is for the dielectric equation and the letter part (**a** through **t**) is for various frequencies and excitations.

4.4.1 Comparing Surface Currents

1. We use the same grid as the PEC case, but since the wavelength inside the dielectric is $1/\sqrt{6}$ the wavelength outside the dielectric, we will lower the frequency in order to obtain the required number of basis functions per wavelength inside the dielectric. We will use the same element pairs to define edges as in the PEC case.

2. Run **jungfrau.** To compare J_θ and J_ϕ we use the same incident wave as we did in the PEC test case. In addition to electric current density, the dielectric sphere has magnetic current density (M). For all surface current calculations we set $\theta_{inc} = 180^0$.

For M_θ we set $\phi_{inc} = 45^0$ and $H_\phi = (+2.65442 \times 10^{-3}, 0.0)$ A/m, which aligns the incident 1 V/m E field 90^0 with respect to the center of the element edges at $\phi_{obs} = 315^0$ and drives the maximum M_θ across these edges. For the analytical solution we will set $\phi_{obs} = 270^0$ to align the observation angle 90^0 with respect to the incident E field.

For M_ϕ we set $\phi_{inc} = 270^0$ and $H_\phi = (+2.65442 \times 10^{-3}, 0.0)$ A/m. This drives the maximum M_ϕ across the edges at $\phi_{obs} = 270^0$. For the analytical solution we set $\phi_{obs} = 0^0$.

3. Run **eiger**. Example input is **sphr_10cm_3a.eig**. Example output is **sphr_10cm_3a.mnh.**

4. Run **moench** asking for unknowns along a line (the ul option) and give the set of element pairs from Step 1 of the PEC case to plot J_θ, J_ϕ, M_θ, or M_ϕ along a constant ϕ value. An example **moench** input file for M_ϕ is **moench_sphr10cm_mp.in,** which is shown in Appendix II. Output is given in a

user-named ***.lin1** file (**sphr_10cm_3c.lin1**, for example).

5. Use a text editor to strip the header information from the *.lin1 file. The zero location of the ***.lin1** file is the first element edge designated in the element pairs, which is not the zero location of the analytical solution. Run **moench_current_offset** to add the proper location offset to the first column of the ***.lin1** file. For J_θ or M_θ we add **0.0945** meters and for J_ϕ or M_ϕ we add **0.0523** meters. An example output file is **mp_10cm3c_offset.txt**. This completes the numerical portion of the comparison.

6. Run **diel_sphere** to obtain the analytic solution. The number of terms (n) is set to be 120 based on the convergence studies in Section 4.3. The frequency of the analytical solution is identical to that of the numerical solution. The radius of the analytic sphere is $a = 0.9989497$ meters. To compare with the numerical solution of J_θ, ϕ_{obs} is set to be 0^0. To compare with the numerical solution of J_ϕ, ϕ_{obs} is set to be 270^0. To compare with the numerical solution of M_θ, ϕ_{obs} is set to be 270^0. To compare with the numerical solution of M_ϕ, ϕ_{obs} is set to be 0^0. The observation radius r_{obs} must be set to be the same as the sphere radius, so $r_{obs} = 0.9989297$ meters. An example input file to calculate M_ϕ (**diel_sphere.in**) is printed in Appendix II. J_θ is output to the file **diel_sphere_jt.txt**, J_ϕ is output to **diel_sphere_jp.txt,** M_θ to **diel_sphere_mt.txt**, and M_ϕ to **diel_sphere_mp.txt**.

7. Run **sphere_surface_compare** to find the point-wise relative error and root mean squared relative error (RE_{rms} given by Equation 3) between the analytical and numerical results.

4.4.2 Comparing Near Fields

Near fields are compared exactly like the PEC case except the analytical solution is found by running **diel_sphere.**

4.4.3 Comparing Far Fields

Far fields are compared exactly like the PEC case except the analytical solution is found by running **diel_sphere.**

4.5 Numerical Results

In Figures 25 through 32, we follow the procedures of Section 4.4 to compare the numerical results to the analytical results. In each figure we compare the magnitude of each quantity of interest computed by **Eiger** (isolated solid triangles) to the quantity calculated analytically (solid lines) as a function of θ. The left hand axis is the magnitude of the quantity. Also plotted in each figure is the relative error (line with open squares), which goes with the right hand axis. All of these results are at $f = 122.38978$ MHz where the elements have an edge length of 1/10 of the wavelength inside the dielectric sphere.

In the tables below we study the RMS relative error for all quantities as we vary the frequency, keeping the grid fixed. The frequency in column 1 along with the nominal size of the element (10cm) yields the number of basis functions per wavelength shown in column 2. The wavelength is that inside the dielectric sphere, ($1/\sqrt{6}$ of the wavelength outside) so the frequency is uniformly lower than the PEC test cases. The remaining columns show the RMS relative error for each quantity of interest.

The table below shows the RE_{rms} for all components of surface current density.

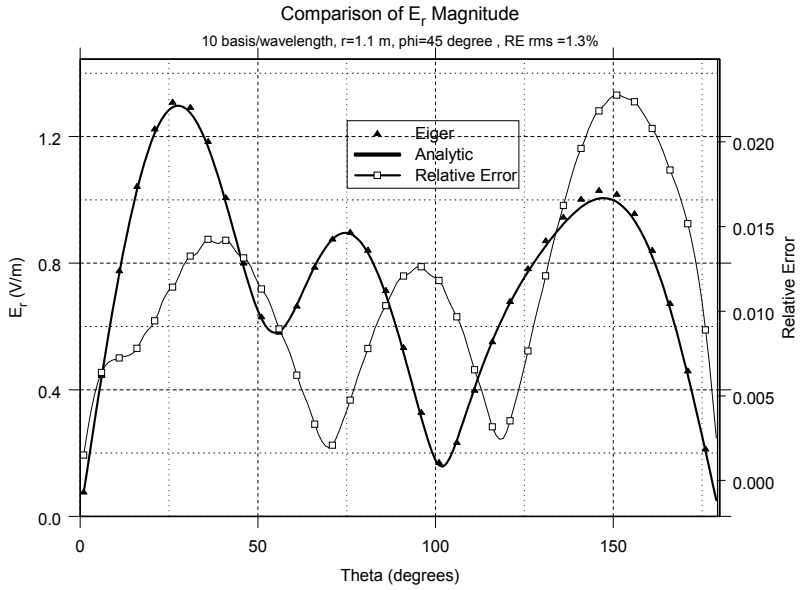

Figure 21. Comparison (left axis) and relative error (right axis) of E_r outside the dielectric sphere vs. θ for $f = 122.38978$ MHz

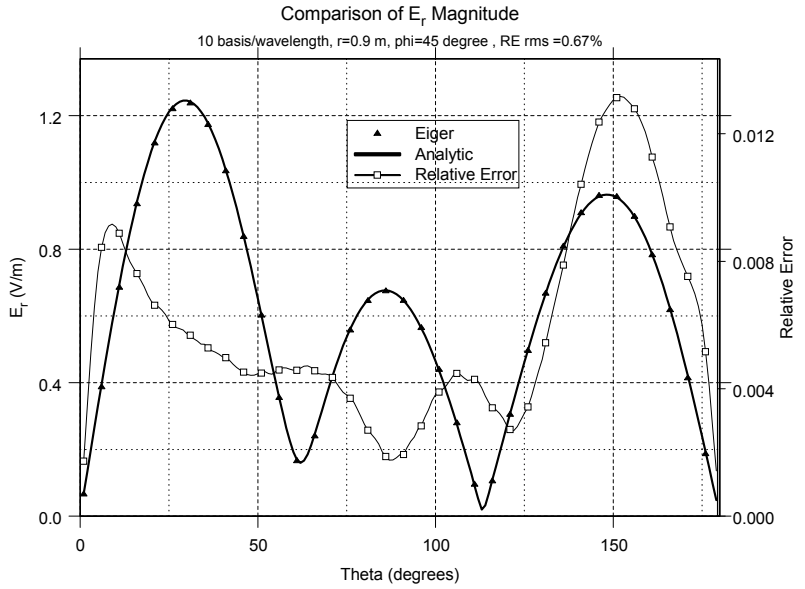

Figure 22. Comparison (left axis) and relative error (right axis) of E_r inside the dielectric sphere vs. θ for $f = 122.38978$ MHz

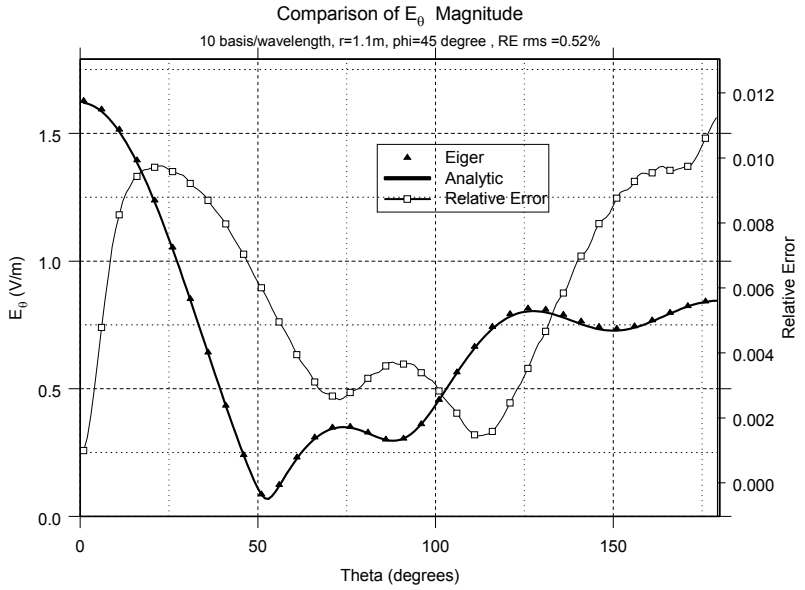

Figure 23. Comparison (left axis) and relative error (right axis) of E_θ outside the dielectric sphere vs. θ for $f = 122.38978$ MHz

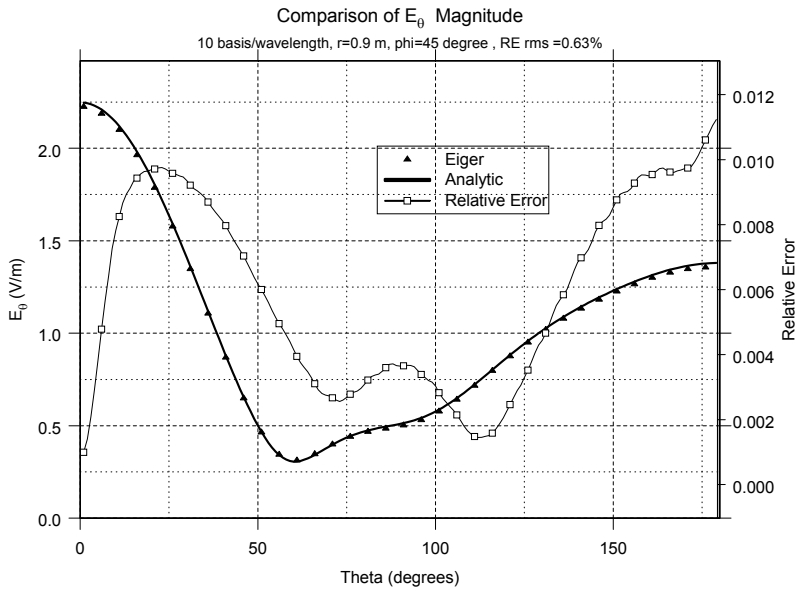

Figure 24. Comparison (left axis) and relative error (right axis) of E_θ inside the dielectric sphere vs. θ for $f = 122.38978$ MHz

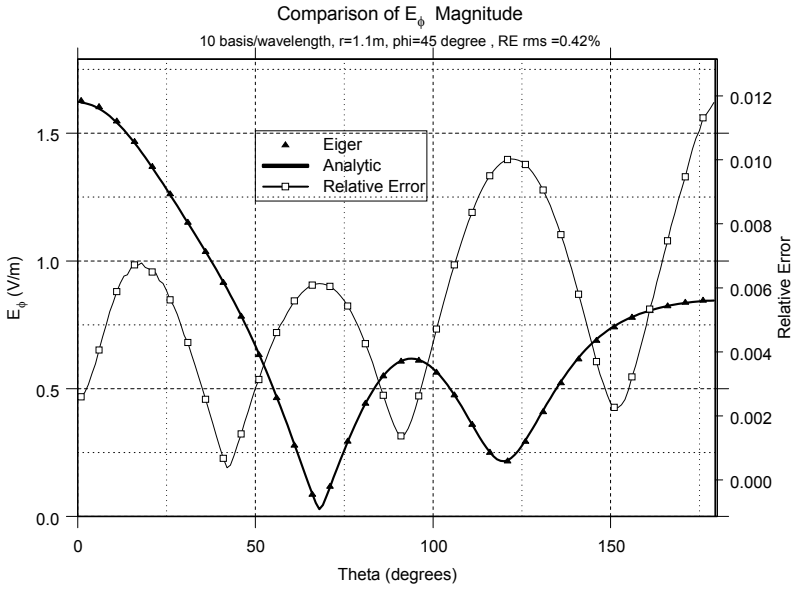

Figure 25. Comparison (left axis) and relative error (right axis) of E_ϕ outside the dielectric sphere vs. θ for $f = 122.38978$ MHz

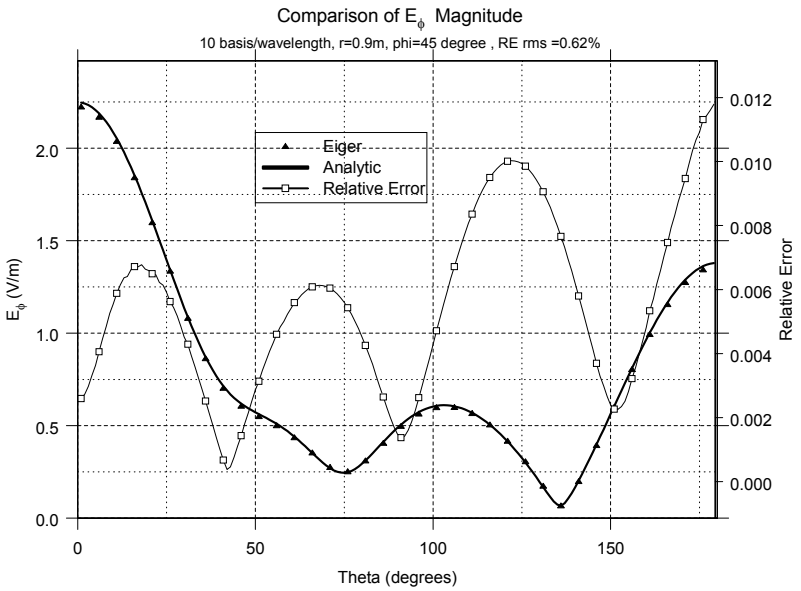

Figure 26. Comparison (left axis) and relative error (right axis) of E_ϕ inside the dielectric sphere vs. θ for $f = 122.38978$ MHz

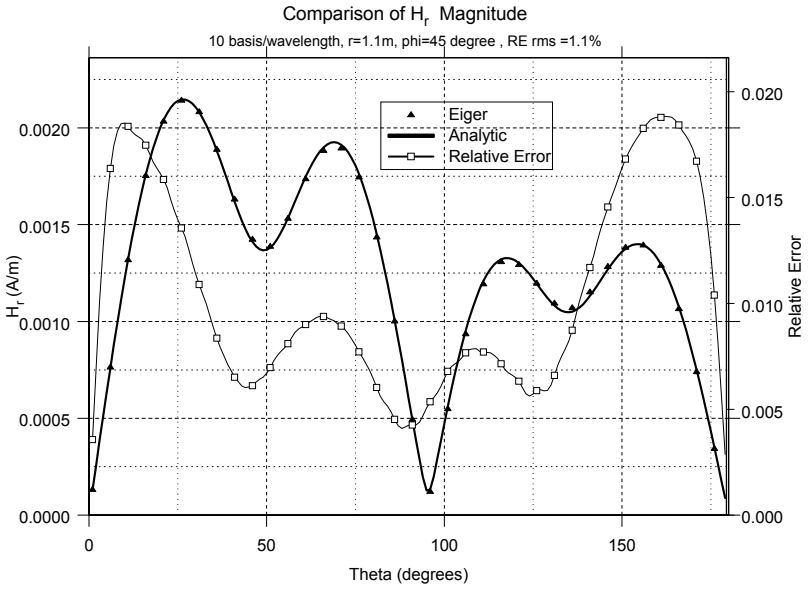

Figure 27. Comparison (left axis) and relative error (right axis) of H_r outside the dielectric sphere vs. θ for $f = 122.38978$ MHz

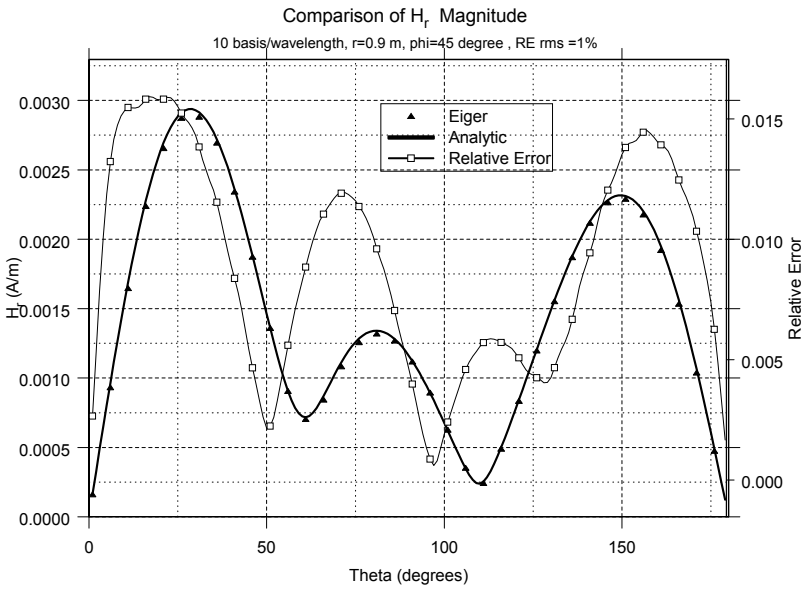

Figure 28. Comparison (left axis) and relative error (right axis) of H_r inside the dielectric sphere vs. θ for $f = 122.38978$ MHz

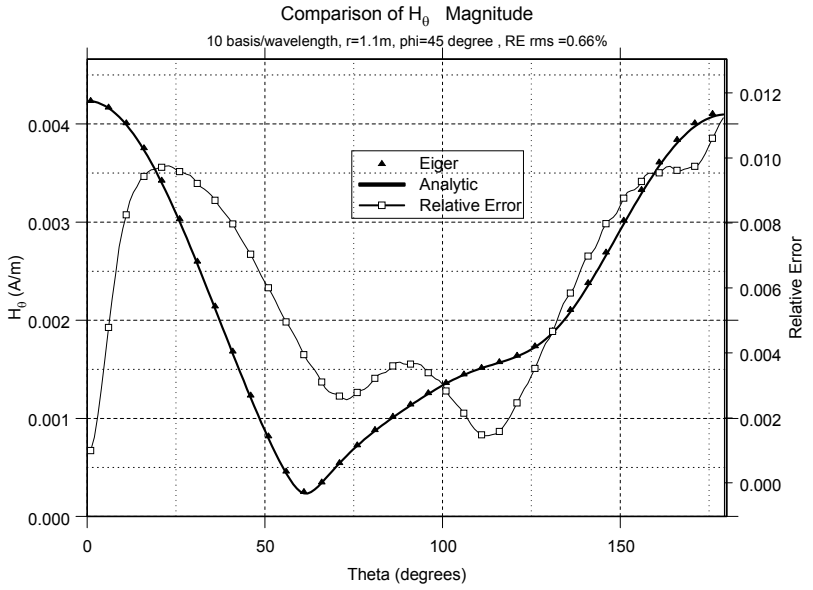

Figure 29. Comparison (left axis) and relative error (right axis) of H_θ outside the dielectric sphere vs. θ for $f = 122.38978$ MHz

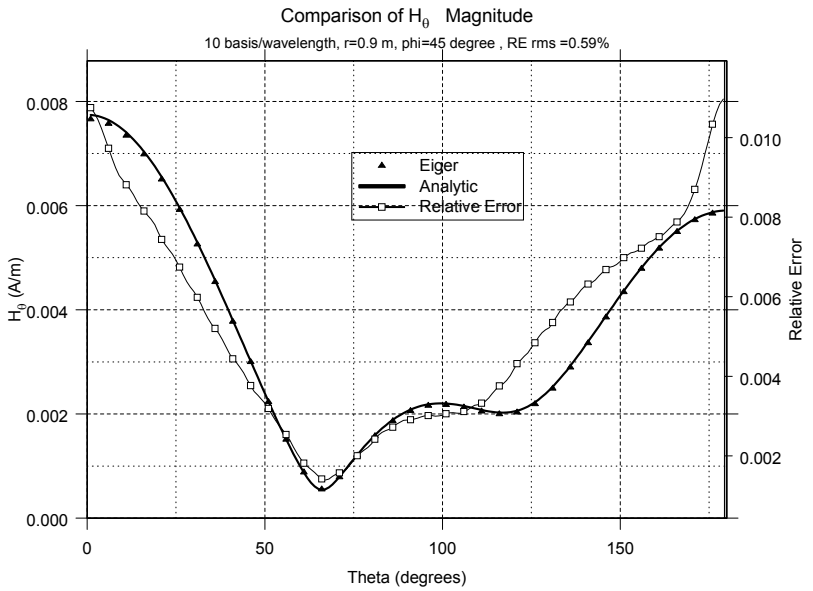

Figure 30. Comparison (left axis) and relative error (right axis) of H_θ inside the dielectric sphere vs. θ for $f = 122.38978$ MHz

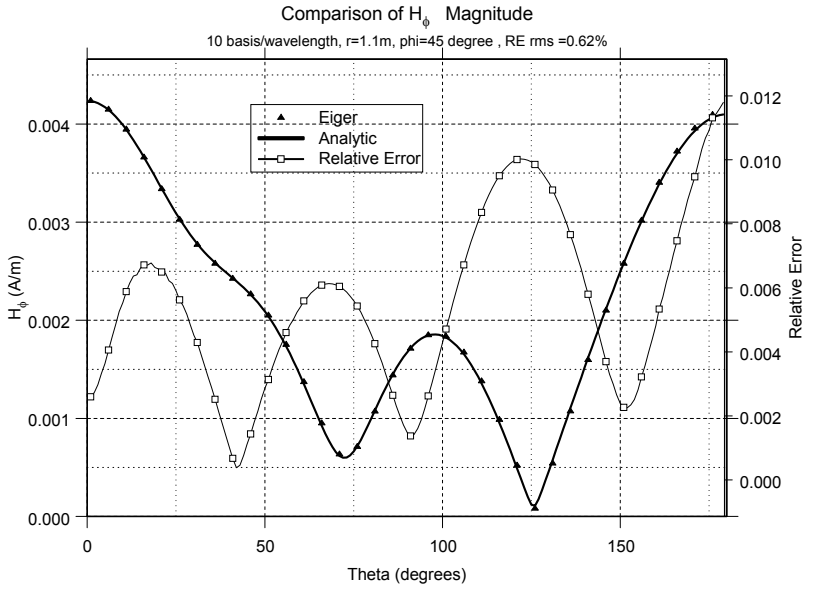

Figure 31. Comparison (left axis) and relative error (right axis) of H_ϕ outside the dielectric sphere vs. θ for $f = 122.38978$ MHz

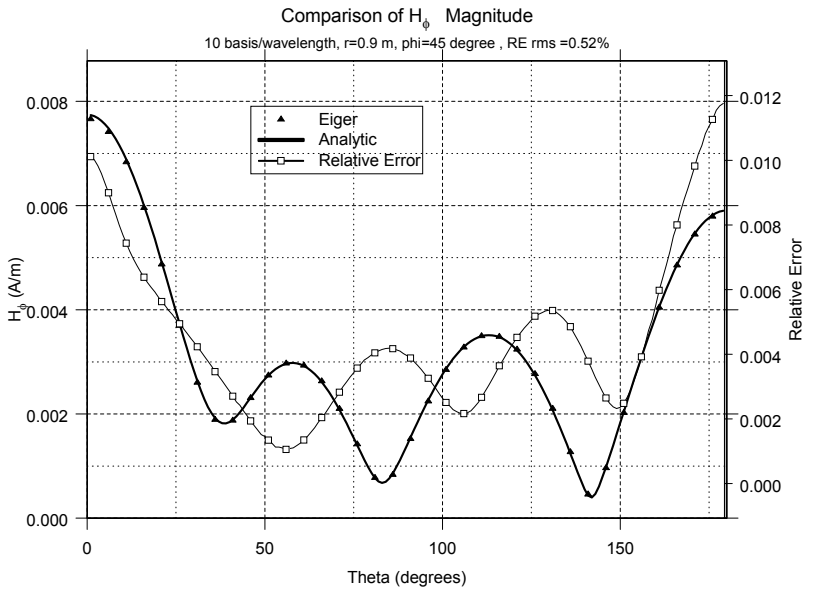

Figure 32. Comparison (left axis) and relative error (right axis) of H_ϕ inside the dielectric sphere vs. θ for $f = 122.38978$ MHz

Frequency (MHz)	basis/λ	J_θ	J_ϕ	M_θ	M_ϕ
12.239	100	0.48×10^{-1}	0.78×10^{-1}	0.55×10^{-1}	0.90×10^{-1}
81.593	15	0.13×10^{-1}	0.14×10^{-1}	0.10×10^{-1}	0.91×10^{-2}
122.390	10	0.11×10^{-1}	0.11×10^{-1}	0.95×10^{-2}	0.11×10^{-1}
174.843	7	0.65×10^{-2}	0.74×10^{-2}	0.53×10^{-2}	0.68×10^{-2}
244.780	5	0.11×10^{-1}	0.10×10^{-1}	0.13×10^{-1}	0.11×10^{-1}

When $r_{obs} = 1.1$ meters (outside the sphere) the RMS errors for the E field components are shown in columns 3 through 5 in the following table. Columns 6 and 7 are the far field errors.

Frequency (MHz)	basis/λ	E_r	E_θ	E_ϕ	E_θ^{ff}	E_ϕ^{ff}
12.239	100	0.60×10^{-2}	0.83×10^{-2}	0.10×10^{-1}	0.12×10^{-2}	0.15×10^{-2}
81.593	15	0.51×10^{-2}	0.54×10^{-2}	0.67×10^{-2}	0.42×10^{-2}	0.47×10^{-2}
122.390	10	0.13×10^{-1}	0.52×10^{-2}	0.42×10^{-2}	0.74×10^{-2}	0.65×10^{-2}
174.843	7	0.71×10^{-2}	0.43×10^{-2}	0.39×10^{-2}	0.32×10^{-2}	0.30×10^{-2}
244.780	5	0.24×10^{-1}	0.11×10^{-1}	0.15×10^{-1}	0.83×10^{-2}	0.10×10^{-1}

The next table shows RMS errors for the H near field at $r_{obs} = 1.1$ m.

Frequency (MHz)	basis/λ	H_r	H_θ	H_ϕ
12.239	100	0.74×10^{-2}	0.76×10^{-2}	0.92×10^{-2}
81.593	15	0.66×10^{-2}	0.50×10^{-2}	0.59×10^{-2}
122.390	10	0.11×10^{-1}	0.66×10^{-2}	0.62×10^{-2}
174.843	7	0.83×10^{-2}	0.38×10^{-2}	0.43×10^{-2}
244.780	5	0.30×10^{-1}	0.10×10^{-1}	0.12×10^{-1}

When $r_{obs} = 0.9$ meters (inside the sphere), the following tables show the errors in the E and H field. The final column is the maximum error found for all other columns.

Frequency (MHz)	basis/λ	E_r	E_θ	E_ϕ
12.239	100	0.21×10^{-1}	0.17×10^{-1}	0.20×10^{-1}
81.593	15	0.15×10^{-1}	0.14×10^{-1}	0.14×10^{-1}
122.390	10	0.67×10^{-2}	0.63×10^{-2}	0.62×10^{-2}
174.843	7	0.11×10^{-1}	0.72×10^{-2}	0.66×10^{-2}
244.780	5	0.18×10^{-1}	0.13×10^{-1}	0.12×10^{-1}

Frequency (MHz)	basis/λ	H_r	H_θ	H_ϕ	Max Error
12.239	100	0.19×10^{-1}	0.15×10^{-1}	0.19×10^{-1}	0.90×10^{-1}
81.593	15	0.16×10^{-1}	0.12×10^{-1}	0.13×10^{-1}	0.16×10^{-1}
122.390	10	0.10×10^{-1}	0.59×10^{-2}	0.52×10^{-2}	0.13×10^{-1}
174.843	7	0.14×10^{-1}	0.56×10^{-2}	0.57×10^{-2}	0.14×10^{-1}
244.780	5	0.23×10^{-1}	0.11×10^{-1}	0.90×10^{-2}	0.30×10^{-1}

Surprisingly, although the errors are small, they do not increase monotonically with frequency as they did in the PEC case. Rather, at 100 basis functions per wavelength the error is less than 9.0%, then it decreases until at 10 basis functions per wavelength the error is less than 1.3% and then it increases again until at 5 basis functions per wavelength it is less than 3%.

5 Lossy Dielectric Sphere Test Case

The equations for the lossy dielectric case are the same as those in Section 4 except that μ_r and ε_r are both complex, with a positive real part and negative imaginary part. The quantities k_d and the Bessel functions are also complex.

5.1 Code Implementation of the Analytical Solution

The formulas in Section 4 were implemented in the code **lossy_sphere.** **Lossy_sphere** calculates quantities of interest versus θ, which varies from 1^0 to 179^0 in 1^0 increments. The other two observation coordinates, ϕ_{obs} and r_{obs}, are set by the user. In the code, $E_0 = 1.0$ V/m.

User input to **lossy_sphere** consists of the following:

- Number of terms used in the summations.
- Frequency (Hertz).
- Relative permittivity of dielectric (unitless).
- Relative permeability of dielectric (unitless).
- Sphere radius a (meters).
- Observation radius r_{obs} (meters).
- Observation phi ϕ_{obs} (degrees).

The results are written to three output files, each of which contain 179 rows (1 row per θ value) and seven columns.

Output files:

- **lossy_sphere_jt.txt**: θ, $|J_\theta|$, phase J_θ, $0.0, 0.0, 0.0, 0.0$
- **lossy_sphere_jp.txt**: θ, $|J_\phi|$, phase J_ϕ, $0.0, 0.0, 0.0, 0.0$
- **lossy_sphere_mt.txt**: θ, $|M_\theta|$, phase M_θ, $0.0, 0.0, 0.0, 0.0$
- **lossy_sphere_mp.txt**: θ, $|M_\phi|$, phase M_ϕ, $0.0, 0.0, 0.0, 0.0$
- **lossy_sphere_enf.txt**: θ, $|E_r|$, phase E_r, $|E_\theta|$, phase E_θ, $|E_\phi|$, phase E_ϕ
- **lossy_sphere_hnf.txt**: θ, $|H_r|$, phase H_r, $|H_\theta|$, phase H_θ, $|H_\phi|$, phase H_ϕ
- **lossy_sphere_ff.txt**: θ, $0.0, 0.0$, $\left|re^{+jkr}E_\theta^{ff}\right|$, phase $re^{+jkr}E_\theta^{ff}$, $\left|re^{+jkr}E_\phi^{ff}\right|$, phase $re^{+jkr}E_\phi^{ff}$

These files are analogous to the output files of **diel_sphere**.

5.2 Convergence Study of the Analytical Solution

We will examine the convergence behavior of the analytical solution as we increase the number of terms. We will use the same parameters as the lossless dielectric sphere except that we will set $\varepsilon_r = (3.0, -0.2)$, and $\mu_r = (2.0, -0.1)$.

For the following tables we will let $R_{exact} = R_{200}$ and then demonstrate that the answer has converged

to eight digits of accuracy (indicated by $\mathrm{RE}_{rms} = 0.0$ in the tables). Each of the table entries gives RE_{rms} (defined in Equation 3) as a function of number of terms (N) for various quantities calculated.

For the low frequency, $f = 2.997925 \times 10^7$ Hz, the analytical solution has converged to eight digits in 20 terms.

N	E_r	E_θ	E_ϕ	E_θ^{ff}	E_ϕ^{ff}
5	0.283×10^{-2}	0.240×10^{-2}	0.205×10^{-2}	0.140×10^{-5}	0.129×10^{-5}
10	0.586×10^{-8}	0.790×10^{-8}	0.372×10^{-8}	0.0	0.0
20	0.0	0.0	0.0	0.0	0.0

N	H_r	H_θ	H_ϕ	Maximum Error
5	0.297×10^{-2}	0.249×10^{-2}	0.211×10^{-2}	0.297×10^{-2}
10	0.548×10^{-8}	0.467×10^{-8}	0.665×10^{-8}	0.790×10^{-8}
20	0.0	0.0	0.0	0.0

For the intermediate frequency, $f = 2.997925 \times 10^8$ Hz, the analytical solution has converged to eight digits in 30 terms.

N	E_r	E_θ	E_ϕ	E_θ^{ff}	E_ϕ^{ff}
10	0.137	0.595×10^{-1}	0.737×10^{-1}	0.136×10^{-2}	0.131×10^{-2}
20	0.136×10^{-6}	0.450×10^{-7}	0.415×10^{-7}	0.0	0.0
30	0.0	0.0	0.0	0.0	0.0

N	H_r	H_θ	H_ϕ	Maximum Error
10	0.152	0.564×10^{-1}	0.688×10^{-1}	0.152
20	0.161×10^{-6}	0.511×10^{-7}	0.420×10^{-7}	0.161×10^{-6}
30	0.0	0.0	0.0	0.0

Finally, for the high frequency, $f = 2.997925 \times 10^9$ Hz, the analytical solution needs 120 terms in order to converge to eight digits.

N	E_r	E_θ	E_ϕ	E_θ^{ff}	E_ϕ^{ff}
50	0.420	0.279	0.278	0.391×10^{-1}	0.394×10^{-1}
70	0.441×10^{-1}	0.222×10^{-1}	0.220×10^{-1}	0.911×10^{-4}	0.890×10^{-4}
90	0.597×10^{-7}	0.337×10^{-7}	0.322×10^{-7}	0.0	0.0
120	0.0	0.0	0.0	0.0	0.0

N	H_r	H_θ	H_ϕ	Maximum Error
50	0.404	0.266	0.300	0.420
70	0.405×10^{-1}	0.202×10^{-1}	0.245×10^{-1}	0.441×10^{-1}
90	0.662×10^{-7}	0.317×10^{-7}	0.279×10^{-7}	0.662×10^{-7}
120	0.0	0.0	0.0	0.0

5.3 Numerical Results

We follow the same procedures as in Section 4.4 to compare the numerical results to the analytical results

Frequency (MHz)	basis/λ	J_θ	J_ϕ	M_θ	M_ϕ
12.239	100	0.48×10^{-1}	0.77×10^{-1}	0.54×10^{-1}	0.89×10^{-1}
81.593	15	0.17×10^{-1}	0.16×10^{-1}	0.12×10^{-1}	0.11×10^{-1}
122.390	10	0.11×10^{-1}	0.12×10^{-1}	0.13×10^{-1}	0.11×10^{-1}
174.843	7	0.12×10^{-1}	0.12×10^{-1}	0.11×10^{-1}	0.11×10^{-1}
244.780	5	0.13×10^{-1}	0.12×10^{-1}	0.14×10^{-1}	0.12×10^{-1}

When $r_{obs} = 1.1$ meters (outside the sphere)

Frequency (MHz)	basis/λ	E_r	E_θ	E_ϕ	E_θ^{ff}	E_ϕ^{ff}
12.239	100	0.60×10^{-2}	0.82×10^{-2}	0.10×10^{-1}	0.11×10^{-2}	0.15×10^{-2}
81.593	15	0.38×10^{-2}	0.41×10^{-2}	0.47×10^{-2}	0.23×10^{-2}	0.24×10^{-2}
122.390	10	0.78×10^{-2}	0.47×10^{-2}	0.52×10^{-2}	0.21×10^{-2}	0.18×10^{-2}
174.843	7	0.63×10^{-2}	0.38×10^{-2}	0.44×10^{-2}	0.12×10^{-2}	0.14×10^{-2}
244.780	5	0.10×10^{-1}	0.55×10^{-2}	0.72×10^{-2}	0.18×10^{-2}	0.30×10^{-2}

Frequency (MHz)	basis/λ	H_r	H_θ	H_ϕ
12.239	100	0.74×10^{-2}	0.75×10^{-2}	0.91×10^{-2}
81.593	15	0.41×10^{-2}	0.39×10^{-2}	0.52×10^{-2}
122.390	10	0.82×10^{-2}	0.39×10^{-2}	0.50×10^{-2}
174.843	7	0.83×10^{-2}	0.38×10^{-2}	0.46×10^{-2}
244.780	5	0.11×10^{-1}	0.59×10^{-2}	0.74×10^{-2}

When $r_{obs} = 0.9$ meters (inside the sphere)

Frequency (MHz)	basis/λ	E_r	E_θ	E_ϕ
12.239	100	0.21×10^{-1}	0.16×10^{-1}	0.20×10^{-1}
81.593	15	0.13×10^{-1}	0.12×10^{-1}	0.12×10^{-1}
122.390	10	0.96×10^{-2}	0.83×10^{-2}	0.82×10^{-2}
174.843	7	0.19×10^{-1}	0.97×10^{-2}	0.97×10^{-2}
244.780	5	0.17×10^{-1}	0.13×10^{-1}	0.13×10^{-1}

Frequency (MHz)	basis/λ	H_r	H_θ	H_ϕ	Max Error
12.239	100	0.19×10^{-1}	0.15×10^{-1}	0.18×10^{-1}	0.89×10^{-1}
81.593	15	0.13×10^{-1}	0.12×10^{-1}	0.12×10^{-1}	0.17×10^{-1}
122.390	10	0.10×10^{-1}	0.97×10^{-2}	0.88×10^{-2}	0.13×10^{-1}
174.843	7	0.19×10^{-1}	0.97×10^{-2}	0.10×10^{-1}	0.19×10^{-1}
244.780	5	0.18×10^{-1}	0.11×10^{-1}	0.11×10^{-1}	0.18×10^{-1}

In terms of convergence as a function of frequency the lossy dielectric sphere behaves much like the lossless dielectric sphere.

6 Conclusions

In this report we demonstrated that **Eiger** can calculate the current density, near fields and far fields for plane wave scattering from three-dimensional objects made of either PEC, lossless dielectric, or lossy dielectric. All available equations were tested. The ability of the CFIE to overcome internal resonance problems was also demonstrated. If the gridding is sufficiently fine (better than 10 basis functions per wavelength) the relative error should be less than the 10% error required by Test 1.a.a. in the EMR

Verification and Validation Plan [1].

7 References

[1] R. E. Jorgenson, W. A. Johnson, L. K. Warne, H. G. Hudson, and B. C. Bedeaux, *EMPHASIS: ASCI Verification and Validation Plan for Electromagnetic Radiation Environment*, SAND2003-2695, July 2003, p. 32.

[2] R. F. Harrington, *Time-Harmonic Electromagnetic Fields*, McGraw Hill Co., New York, 1961 pp. 292-298.

[3] M. Abramowitz and I. A Stegun, *Handbook of Mathematical Functions*, Dover Publications, Inc., New York 1965.

[4] SLATEC Common Mathematical Library, Version 4.1 available at **www.netlib.org/slatec,** July 1993.

8 Appendix I: Special Functions

8.1 Associated Legendre Polynomials $P_n^1(x)$

For the calculations discussed in this report, the order of the associated Legendre polynomial is always 1 and degree is an integer, $n = 1...N$. The results will be stored in the array P1(n) where n represents the degree. The first two values in the sequence are calculated explicitly.

$$P1(1) = P_1^1(x) = -\left(1 - x^2\right)^{1/2}$$

$$P1(2) = P_2^1 = -3x\left(1 - x^2\right)^{1/2}$$

The remaining values, $n = 3...N$, are calculated using a recursion relation [3].

$$(n + 1 - m) R_{n+1}^m(x) - (2n + 1) x R_n^m(x) + (n + m) R_{n-1}^m(x) = 0$$

Let $m = 1$

$$\begin{aligned} R_{n+1}^1(x) &= \frac{(2n+1)}{n} x R_n^1(x) - \frac{(n+1)}{n} R_{n-1}^1(x) \\ P1(n+1) &= \frac{2n+1}{n} x P1(n) - \frac{n+1}{n} P1(n-1) \end{aligned}$$

We checked the result using tables found in [3].

8.2 First Derivative of Associated Legendre Polynomials $P_n^{1\prime}(x)$

Again the order is always 1 and degree is an integer 1 to N. The results will be stored in an array $DP1(n)$ where n represents the degree.

$$\frac{dP_n^m(x)}{dx} = \frac{1}{1-x^2}\left[-nxP_n^m(x) + (n+m)\,P_{n-1}^m(x)\right]$$

Let $m = 1$, therefore,

$$\begin{aligned}\frac{dP_n^1(x)}{dx} &= \frac{1}{1-x^2}\left[-nxP_n^1(x) + (n+1)\,P_{n-1}^1(x)\right] \\ DP1(n) &= \frac{1}{1-x^2}\left[-xnP1(n) + (n+1)\,P1(n-1)\right]\end{aligned}$$

For the special case of $n = 1$

$$\begin{aligned}\frac{dP_1^1(x)}{dx} &= \frac{x}{(1-x^2)^{1/2}} \\ DP1(1) &= \frac{x}{(1-x^2)^{1/2}}\end{aligned}$$

We checked the above result against a finite-difference approximation of the derivative using $P_n^1(x)$.

8.3 Alternative Spherical Bessel Functions $\widehat{B}_n$

The alternative spherical Bessel function of order n is

$$\widehat{B}_n(x) = \sqrt{\frac{\pi x}{2}}B_{n+1/2}(x)$$

where B_n represents the Bessel function of the first or second kind, and $n = 1$ to N. $B_{n+1/2}(x)$ is calculated using the SLATEC [4] routines BESJ or BESY and stored in $B1(n)$. We checked the result using tables found in [3].

8.4 First Derivative of Alternative Spherical Bessel Function $\widehat{B}'_n$

$$\begin{aligned}\frac{d\widehat{B}_n(x)}{dx} &= -\sqrt{\frac{\pi x}{2}}B_{n+1+1/2}(x) + \left(\sqrt{\frac{\pi}{2x}}(n+1)\right)B_{n+1/2}(x) \\ DB1(n) &= -\sqrt{\frac{\pi x}{2}}B1(n+1) + \left(\sqrt{\frac{\pi}{2x}}(n+1)\right)B1(n)\end{aligned}$$

We checked the derivative against a finite difference approximation of $\widehat{B}'_n$ using $\widehat{B}_n$.

8.5 Second Derivative of Alternative Spherical Bessel Function $\widehat{B}''_n$

$$\begin{aligned}\frac{d^2\widehat{B}_n(x)}{dx^2} &= \sqrt{\frac{\pi x}{2}}B_{n+2+1/2}(x) - \sqrt{\frac{\pi}{2x}}(2n+3)\,B_{n+1+1/2}(x) + \sqrt{\frac{\pi}{2x^3}}(n+1)\,nB_{n+1/2}(x) \\ DB2(n) &= \sqrt{\frac{\pi x}{2}}B1(n+2) - \sqrt{\frac{\pi}{2x}}(2n+3)\,B1(n+1) + \sqrt{\frac{\pi}{2x^3}}(n+1)\,nB1(n)\end{aligned}$$

We checked the second derivative against a finite difference approximation of $\widehat{B}_n''$using $\widehat{B}_n'$.

9 Appendix II - Example Input Files

9.1 Electric Current Density

The following input to **jungfrau (sphr_10cm_0a.in)** is used to obtain an *.eig file for the PEC sphere in order to calculate J_θ, E_n, all components of E and H in the near field and E in the far field.

```
continue
continue
ce                                  ! create an *.eig file option
sphere_10cm                         ! *.jfg file (input)
sphr_10cm_0a                        ! *.eig file (output)
ya                                  ! overwrite all
1 meter radius, 10cm edge, PEC sphere, theta=180, phi=315, f=2.997925e7
3 dimensional problem
dynamic problem
no ground planes
no periodicity
meter
body1                               ! green property
sm                                  ! solid metal
pec                                 ! material of sphere
efie                                ! equation
linear                              ! interpolation order
away                                ! element normals point away from metal
1                                   ! region surrounding metal
no symmetry
continue
homogeneous                         ! region 1 definition
(1.0,0.0)                           ! relative permittivity
(1.0,0.0)                           ! relative permeability
continue
no movement
0 lumped loads
ot                                  ! excitations defined one at a time
1                                   ! one excitation defined
plane wave                          ! the excitation is a plane wave
ot                                  ! the plane waves are defined one at a time
1                                   ! 1 plane wave is defined
1                                   ! plane wave is in region 1
180.0                               ! theta value
315.0                               ! phi value
(0.0,0.0)                           ! H theta
(+2.65442e-3,0.0)                   ! H phi
ot                                  ! frequencies one at a time
1                                   ! one frequency
2.997925e7                          ! frequency
```

```
bl                                  ! blanket solutions
lu                                  ! LU decomposition
0                                   ! 0 far field patterns
58                                  ! E normal defined at 58 elements
2168                                ! Element 1
2146                                ! Element 2
2145
2116
2115
2086
2085
2056
2055
2026
2025
1996
1995
1966
1965
1936
1935
1906
1905
1876
1875
1846
1845
1816
1815
1786
1785
1756
1755
15
16
45
46
75
76
105
106
135
136
165
166
195
196
225
226
255
256
285
```

```
286
315
316
345
346
375
376
405
406
428                                  ! Element 58
```

The following input to **moench (moench_sphr10cm_jt.in)** writes the unknowns associated with J_θ along a line defined by the user.

```
sphr_10cm_0a      *.eig file  (input)
sphr_10cm_0a      *.mnh file  (input)
ul                unknowns along a line option
sphr_10cm_0a      *.lin1 file (output)
ya                overwrite all
1                 frequency id
1                 excitation id
exit              exit information loop
1 1               node_set_id 1, unknown_id 1 (electric current)
29                number of element pairs
2168              pair 1
2146
2145              pair 2
2116
2115              pair 3  etc...
2086
2085
2056
2055
2026
2025
1996
1995
1966
1965
1936
1935
1906
1905
1876
1875
1846
1845
1816
1815
1786
1785
1756
```

```
1755
15
16
45
46
75
76
105
106
135
136
165
166
195
196
225
226
255
256
285
286
315
316
345
346
375
376
405
406              pair 29
428
quit             quit moench
```

The following input to **pec_sphere** is to compare J_θ. Note that the $\phi_{obs} = 0.0$.

```
50                number of terms
29.97925e+06      frequency
0.9989497         sphere radius
0.9989497         observation radius
0.0               observation phi
```

9.2 Near Fields

The following input to **moench (moench_sphr1.1_nfld.in)** is to calculate the near field along an arc defined by the *.jfg file **sphere_1p1_0d**. Note that the *.eig file used here must be the same as the *.eig file used to generate the *.mnh file. If the *.eig file used here is for a different excitation or frequency, the near fields will be incorrect.

```
sphr_10cm_3a             *.eig file
sphr_10cm_3a             *.mnh file
nf                       near field option
re                       read in grid
```

```
1                       region
sphere_1p1_0d           *.jfg grid for near fields
yes                     output a near field for this excitation
sphr_10cm3a_r1.1_0deg   name of near field file
ya                      overwrite existing file
quit                    quit moench
```

The following input to **pec_sphere** is to compare near fields. Note that the $\phi_{obs} = 45^0$ and $r_{obs} = 1.1$ meters

```
120              number of terms
29.97925e+06     frequency
0.9989497        sphere radius
1.1              observation radius
45.0             observation phi
```

9.3 Far Fields

The following input to **moench (moench_sphr10cm_ffld.in)** is to calculate the far field along an arc defined by the user. Note that the *.eig file used here must be the same as the *.eig file used to generate the *.mnh file. If the *.eig file used here is for a different excitation or frequency, the far fields will be incorrect.

```
sphr_10cm_3a          *.eig
sphr_10cm_3a          *.mnh
ff                    far field option
1                     number of far_field patterns
1                     region id
179                   number angles in theta
1.0                   first theta angle
179.0                 last theta angle
1                     number of angles in phi
0.0                   phi angle
yes                   make a plot for excitation and frequency
sphr10cm3e_ff_0deg    far field file
ya                    overwrite the old files
quit                  quit moench
```

9.4 Magnetic Current Density

The following input to moench (**moench_sphr10cm_mp.in)** writes the unknowns associated with M_ϕ along a line defined by the user.

```
sphr_10cm_3d     *.eig file (input)
sphr_10cm_3d     *.mnh file (input)
ul               unknowns along a line option
sphr_10cm_3d     *.lin1 file (output)
ya               overwrite all
1                frequency id
1                excitation id
```

```
exit              exit the information loop
1 2               node_set_id 1, unknown_id 2 (magnetic current)
30                number of element pairs
2596              pair 1
2175
2566              pair 2
2160
2536              pair 3 etc...
2130
2506
2100
2476
2070
2446
2040
2416
2010
2386
1980
2356
1950
2326
1920
2296
1890
2266
1860
2236
1830
2206
1800
2176
1770
465
1
495
31
525
61
555
91
585
121
615
151
645
181
675
211
705
241
735
```

```
271
765
301
795
331
825
361
855
391
870               pair 30
421
quit              quit moench
```

The following input to **diel_sphere** is to compare M_ϕ. Note that the $\phi_{obs} = 0.0$ and r_{obs} equals the radius of the sphere.

```
50                number of terms
12.23898E+06      frequency
3.0               epsilon
2.0               mu
0.9989497         sphere radius
0.9989497         observation radius
0.0               observation phi
```

Distribution:

3	MS1152	R. E. Jorgenson, 01642
3	MS1152	J. D. Kotulski, 01642
1	MS1152	R. S. Coats, 01642
1	MS1152	W. A. Johnson, 01642
1	MS1152	L. I. Basilio, 01642
1	MS1152	M. L. Kiefer, 01642
1	MS0139	S. E. Lott, 09905
1	MS0828	M. Pilch, 09133
1	MS0370	T. G. Trucano, 09211
1	MS9018	Central Technical Files, 8945-1
2	MS0899	Technical Library, 09616
1	MS0612	Review & Approval Desk, 09612 For DOE/OSTI